

ZK-HybridFL: Zero-Knowledge Proof-Enhanced Hybrid Ledger for Federated Learning

*Amirhossein Taherpour, and *Xiaodong Wang, Fellow, IEEE

*Electrical Engineering Department, Columbia University

at3532@columbia.edu, xw2008@columbia.edu

Abstract—Federated learning (FL) enables collaborative model training while preserving data privacy, yet both centralized and decentralized approaches face challenges in scalability, security, and update validation. We propose ZK-HybridFL, a secure decentralized FL framework that integrates a directed acyclic graph (DAG) ledger with dedicated sidechains and zero-knowledge proofs (ZKPs) for privacy-preserving model validation. The framework uses event-driven smart contracts and an oracle-assisted sidechain to verify local model updates without exposing sensitive data. A built-in challenge mechanism efficiently detects adversarial behavior. In experiments on image classification and language modeling tasks, ZK-HybridFL achieves faster convergence, higher accuracy, lower perplexity, and reduced latency compared to Blade-FL and ChainFL. It remains robust against substantial fractions of adversarial and idle nodes, supports sub-second on-chain verification with efficient gas usage, and prevents invalid updates and orphanage-style attacks. This makes ZK-HybridFL a scalable and secure solution for decentralized FL across diverse environments.

Index Terms—Federated learning (FL), decentralized machine learning, distributed ledger technology (DLT), blockchain, directed acyclic graph (DAG), zero-knowledge proofs (ZKPs), privacy-preserving machine learning.

I. Introduction

FEDERATED learning (FL) has emerged as a promising paradigm for collaboratively training models across distributed data silos while preserving privacy [1]. However, traditional FL architectures typically rely on centralized coordinators, potentially creating single points of failure and trust bottlenecks [2]. To overcome these limitations, decentralized FL frameworks have been proposed that leverage distributed ledger technologies (DLTs) for trustless coordination [3].

A variety of blockchain-based approaches illustrate the potential of decentralizing FL. For instance, BlockFL [4] optimizes secure model exchanges and rewards by adjusting the block generation rate, while PIRATE [5] implements a sharding-based design to achieve Byzantine resilience through secure gradient aggregation. Other notable efforts include adaptive FL methods that reduce communication overhead by up to 50% [6], incentive mechanisms grounded in reputation systems [7], proof-of-stake (PoS)-based resource-saving algorithms [8], Top- k compression for limiting communication costs [9], and blockchain-empowered frameworks for 5G-enabled unmanned aerial vehicles (UAVs) [10]. Further studies have

analyzed energy consumption in blockchain networks [11], latency optimization [4], and integration with mobile edge computing [12], while foundational research has established theoretical bounds for resource-constrained FL settings [13] and proposed reputation-oriented incentive schemes for preserving Internet of Things (IoT) data privacy [14].

Despite these advances, significant obstacles remain. Current frameworks often struggle to balance scalability, security, and privacy when operating at scale or in diverse, adversarial environments [15]. Synchronous systems (e.g., those relying on Proof of Work (PoW) or Practical Byzantine Fault Tolerance (PBFT)) can become bottlenecks under straggler nodes, while solutions that rely on public datasets for validation risk data exposure and fail to accommodate the heterogeneity of real-world data [16], [17], [18]. Moreover, advanced gradient inversion techniques [19], label inference attacks [20], and disaggregation methods [21] highlight the difficulty of protecting participant information purely through naive data-sharing defenses. Although differential privacy [22] can mitigate certain risks, it does not resolve the fundamental challenge of publicly verifying the integrity of local model updates at scale [23].

A. State-of-the-Art and Challenges

Blade-FL [24] removes the need for a centralized server by integrating blockchain directly into the FL workflow. In each epoch, nodes train their local models on mini-batches, then sign and broadcast the updates as blockchain transactions. These updates are verified against a public dataset based on a loss threshold and are aggregated—by averaging the validated updates—into a global model. Subsequently, nodes compete to mine a new block via PoW, which records both the verified transactions and the aggregated model. Once the block is validated network-wide, the updated global model is adopted for the next training round. This cycle repeats until convergence.

ChainFL [25] adopts a hierarchical blockchain structure of node, subchain, and mainchain layers to facilitate FL without a central server. A task is initiated via a smart contract on a DAG ledger, broadcasting the request across shards. Within each shard, the Subchain Leader Node (SLN) distributes the current global model to participating nodes, collects their locally trained updates, and aggregates them—weighted by dataset sizes—using the Raft

consensus mechanism before committing the aggregated result to that shard’s blockchain. The SLN then submits this shard-level model to the DAG, where top models from different shards are evaluated on a public dataset to form the next global model. This iterative process of local training, aggregation, and cross-shard validation continues until the smart contract conditions signal completion of the FL task.

Both Blade-FL and ChainFL introduce valuable decentralization strategies but face critical limitations in practice. Blade-FL’s reliance on PoW leads to heavy computational overhead and high energy consumption, while the use of a public validation dataset raises privacy concerns and risks adversarial manipulation. ChainFL’s hierarchical, sharded structure, though beneficial for scaling, still depends on centralized public dataset evaluations and suffers from cross-shard synchronization overhead that can allow stale or malicious updates to proliferate. Motivated by these shortcomings, our work proposes a novel framework that integrates a DAG-based ledger with sidechains and employs zero-knowledge proofs (ZKPs) for privacy-preserving, on-device model validation. This approach not only eliminates the need for public datasets but also boosts efficiency and scalability by ensuring only genuine, high-quality updates are accepted into the global model.

At a broader level, existing solutions also highlight the unmet need for robust and efficient methods of verifying local model updates without compromising user data. Conventional methods often resort to public datasets for legitimacy checks [16], [26], exposing privacy vulnerabilities and undermining real-world representativeness. Advanced cryptographic protocols, such as ZKPs [27], can address privacy and correctness simultaneously, but current implementations often support only specific model types (e.g., linear regression [28]) or suffer from high computational overheads [29]. These drawbacks underscore the need for a more scalable, generalizable solution that keeps participant data private while enabling secure, public verification of model contributions.

In this paper, we introduce ZK-HybridFL, a novel decentralized FL architecture that addresses these gaps through an innovative ledger design and cryptographic validation pipeline. Our framework combines a DAG for high-throughput storage of model updates with sidechains dedicated to Event-Driven Smart Contracts (EDSCs). By embedding ZKPs in the sidechain-based contracts, we create a method for verifying training correctness without disclosing sensitive information, thereby eliminating the overhead and security pitfalls of traditional solutions.

B. Contributions

- Our primary contributions are as follows:
- 1) **Hybrid Ledger System:** We propose a DAG-based ledger for scalable storage of model updates, augmented by sidechains running EDSCs to manage consensus and validation tasks. This structure alleviates bottlenecks inherent in purely PoW- or DAG-based systems.

- 2) **ZKP-Driven Secure Validation:** By integrating ZKPs into EDSCs, our framework enables public verification of inference correctness without exposing private test data or imposing prohibitive computational costs.
- 3) **Experimental Validation:** Through extensive simulations, we demonstrate that our approach outperforms Blade-FL [24] and ChainFL [25] in accuracy, convergence speed, and resilience, even in the presence of adversarial or lazy nodes.

The remainder of the paper is organized as follows. Sec. II introduces the ZKP-based consensus mechanism and DAG ledger for decentralized FL. Sec. III describes the event-driven smart contracts and oracle-assisted sidechain. Sec. IV outlines the ZK-HybridFL workflow and analysis. Sec. V presents simulation results and comparisons with existing schemes, and Sec. VI concludes the paper with future research directions.

II. ZKP-based Consensus Mechanism of ZK-HybridFL

In this section, we first present the use of zero-knowledge proofs (ZKPs) for privacy-preserving model validation. Next, we explain the directed acyclic graph (DAG) ledger, which manages scalable and decentralized model updates. Finally, we discuss the challenge mechanism for verifying blocks and resolving conflicts to ensure system integrity.

A. ZKP

- 1) **Motivation of using private data for model validation:** When selecting between a public test dataset and private test datasets secured via ZKP in decentralized federated learning (FL), opting for private test datasets offers significant advantages in both privacy and model quality. Utilizing a public test dataset simplifies evaluation by providing a uniform benchmark for all nodes, which facilitates straightforward comparisons. However, the public and static nature of such datasets may result in models being validated on a limited variety of unseen data, potentially restricting their robustness and adaptability [22]. Additionally, as nodes continuously refine their local models to perform well on the public test set, the evolving patterns in their loss or accuracy can inadvertently expose information about their private training data through techniques such as membership inference or model inversion [30], [31]. In contrast, employing private test datasets with ZKPs ensures that each local model is assessed using diverse and private test samples. This approach enhances exposure to a broader data distribution, thereby improving the global model’s quality and generalizability while simultaneously protecting data privacy.

- 2) **The ZKP process:** A ZKP is a cryptographic technique that enables one party (the prover) to convince another party (the verifier) of the validity of a statement without revealing any information beyond the fact that the statement is valid. In computation-related applications, the prover and verifier agree on a specific algorithm or function. The goal is for the prover to demonstrate to the verifier that the output of the algorithm or function is

indeed the result of a particular input, without disclosing any additional details about the input or process.

In ZK-HybridFL, ZKPs enable a node j (prover) to demonstrate to other nodes j' (verifiers) that its inference output \mathcal{Y}_j^t at time step t is correctly derived by applying its publicly available model \mathbf{W}_j^t , trained during epoch t , to its private test batch $\mathcal{D}_j^{t,\text{test}}$ using the inference algorithm \mathcal{I} without revealing any details about $\mathcal{D}_j^{t,\text{test}}$ or the internal computations. Recall that each node j maintains a local dataset \mathcal{D}_j^t , and a training mini-batch $\mathcal{D}_j^{t,\text{train}}$ is used to obtain the model \mathbf{W}_j^t . The test mini-batch $\mathcal{D}_j^{t,\text{test}}$ is drawn from the remaining data, i.e., $\mathcal{D}_j^{t,\text{test}} \subset \mathcal{D}_j^t \setminus \mathcal{D}_j^{t,\text{train}}$.

To achieve ZKP, a predefined, immutable program called the circuit is created based on the given inference algorithm \mathcal{I} . Once compiled, this circuit executes a sequence of unforgeable operations that generate both the predicted output \mathcal{Y}_j^t and its associated loss value $\mathcal{L}(\mathcal{D}_j^{t,\text{test}}, \mathcal{Y}_j^t)$, which measures the quality of the model \mathbf{W}_j^t . In the process, it produces explicitly defined, immutable intermediate results, referred to as witnesses and denoted by \mathcal{U}_j^t . To ensure the integrity of this computation, a verifier must check the consistency of the inputs $\mathcal{D}_j^{t,\text{test}}$ and \mathbf{W}_j^t , the intermediate results \mathcal{U}_j^t , and the outputs \mathcal{Y}_j^t and $\mathcal{L}(\mathcal{D}_j^{t,\text{test}}, \mathcal{Y}_j^t)$. In particular, the prover node j and the verifier node j' follow the sequence of actions outlined below:

- 1) Commit: At the beginning of epoch t , the trainer binds both its freshly trained weight tensor \mathbf{W}_j^t and its private test batch $\mathcal{D}_j^{t,\text{test}}$ by posting polynomial commitments

$$C_j^{t,\text{model}} = \text{Commit}(\mathbf{W}_j^t), \quad C_j^{t,\text{test}} = \text{Commit}(\mathcal{D}_j^{t,\text{test}})$$

to the sidechain.¹

- 2) Key availability: A one-time powers-of-tau ceremony (run off-chain by the oracle committee) produces a circuit-specific proving key pk and a public verification key vk . Because the inference circuit is fixed for the entire task, pk and vk are reused by every node and for every epoch; only the private witness $(\mathbf{W}_j^t, \mathcal{D}_j^{t,\text{test}})$ changes.
- 3) Proof generation: Using the proving key pk and its private witness $(\mathbf{W}_j^t, \mathcal{D}_j^{t,\text{test}})$, node j evaluates the circuit to obtain \mathcal{U}_j^t (the full witness) and the public outputs \mathcal{Y}_j^t and \mathcal{L}_j^t . It then computes the non-interactive Groth16 proof

$$\Pi_j^t = \text{Prove}(\text{pk}, \mathcal{U}_j^t),$$

where all Fiat–Shamir challenges are derived deterministically from $\text{H}(\text{blockHash} \parallel C_j^{t,\text{model}} \parallel C_j^{t,\text{test}})$, so no live randomness exchange is needed. Finally, trainer j broadcasts

$$Z_j^t = (\Pi_j^t, \mathcal{Y}_j^t, \mathcal{L}_j^t, C_j^{t,\text{model}}, C_j^{t,\text{test}}).$$

¹A simple hash is sufficient at this stage; Sec. S1-A1 gives the concrete KZG instantiation and its 35 k gas verification cost.

- 4) Verification: Any verifier j' fetches the verification key vk from the sidechain and checks

$$\text{Verify}(\text{vk}, \Pi_j^t, C_j^{t,\text{model}}, C_j^{t,\text{test}}, \mathcal{Y}_j^t, \mathcal{L}_j^t) = 1.$$

A result of 1 certifies that the public outputs \mathcal{Y}_j^t and \mathcal{L}_j^t were produced exactly by the committed model and test data; otherwise, the update is rejected. Once verification succeeds, a ProofOK event is emitted, allowing the contribution to enter the DAG.

A detailed cryptographic instantiation, including the polynomial-commitment scheme and trusted setup, is given in the supplementary material (Sec. S1-A1). The keys pk and vk are fixed across nodes and epochs, while each proof Π_j^t is specific to its witness. Completeness, soundness, and zero-knowledge follow from the Groth16 construction (see Sec. S1-A2).

Remark II.1. ZKPs are generally categorized into two main types: succinct non-interactive arguments of knowledge (SNARKs) and scalable transparent arguments of knowledge (STARKs). In our scheme, we utilize ZK-SNARKs due to their succinct proofs, efficient verification, and compatibility with blockchain-based systems. SNARKs such as Groth16 [32] and Pinocchio [33] rely on elliptic-curve cryptography and a trusted setup, which is effectively managed in our scheme by an oracle. While STARKs offer advantages such as transparency (no trusted setup) and post-quantum security, their larger proof sizes and higher computational costs make them less practical in our context. For a detailed discussion of these ZKP methods, see [34], [35].

Remark II.2. To prevent proof-generation latency from inflating overall training time, ZK-HybridFL employs a predict-then-prove workflow. Immediately after completing a local training step, each node (i) broadcasts its model update together with its hash, and then (ii) proceeds with the next stochastic gradient descent (SGD) iteration without waiting for the zero-knowledge proof to be produced. Proofs are generated asynchronously in the background and thus are effectively amortized over subsequent training steps. A two-epoch (configurable) grace period is provided before any proof failures trigger the challenge mechanism, ensuring that transient delays do not stall the protocol under normal hardware conditions.

While the core ZKP workflow verifies inference correctness, it does not prevent subtler “stealth” attacks, such as submitting trivially small or semantically unchanged updates. We develop extended ZKP defenses to counter these threats. A formal security analysis of these defenses is presented in the supplementary material (Sec. S1-C), with empirical validation provided by detailed simulations (Sec. S3-C2).

B. DAG

By using a modified IOTA Coordicide consensus mechanism [36] as described next, ZK-HybridFL employs a DAG ledger to facilitate interactions among trainer nodes while keeping the overall network scalable and secure.

The basic DAG operations used in ZK-HybridFL, such as tip-based parent selection, weight accumulation for confirmation, and graph reachability checks that support the challenge process, are adopted almost verbatim from the Coordicide design of the IOTA ledger.

Our contributions lie in how these established primitives are repurposed for FL. First, every block must include a ZKP that is verified on-chain before the block can gain any weight. This guarantees that only correctly trained updates can influence the ledger. Second, the loss-aware aggregation policy (Sec. III-A4) admits only the most recent confirmed blocks and ranks candidate parents by their validated loss. As a result, low-quality or adversarial updates accrue insufficient weight and are naturally pruned from the ledger. To the best of our knowledge, no prior DAG-based blockchain combines proof-gated admission with loss-aware parent selection in the context of a decentralized parameter server. This dual gating mechanism is the core algorithmic contribution of ZK-HybridFL’s DAG layer.

In our proposed scheme, each node j submits a block $D_j(t) = [\mathbf{W}_j^t, Z_j^t]$ to the DAG ledger during epoch t , where \mathbf{W}_j^t is the updated local model and Z_j^t is the ZKP bundle described in Sec. II-A. Blocks $D_j(t)$ within the DAG can exist in one of three states: confirmed, tip, or unconfirmed. Confirmed blocks $D_j^C(t)$ have an aggregated weight (AW) exceeding a predefined threshold, making them validated and integrated into the stable, immutable part of the DAG. Tip blocks $D_j^T(t)$ are the most recent blocks at the DAG’s frontier, ready to be extended by incoming blocks. Unconfirmed blocks $D_j^U(t)$ are those added to the DAG but still in a pending state, awaiting sufficient AW to reach confirmation.

During each epoch t , the global model $\tilde{\mathbf{W}}_j^t$ is obtained through local model aggregation using the model updates from the most recently confirmed blocks, as detailed in Sec. III-A4. Next, we provide a detailed explanation of the consensus mechanism for the DAG component and the computation of the AW used for block confirmation within the DAG.

To submit its contributed block $D_j(t)$ for epoch t to the DAG, node j begins by randomly selecting K_T tip blocks. These chosen blocks form a set $\mathcal{D}_j^T(t)$ of potential parents with $|\mathcal{D}_j^T(t)| = K_T$. For each block $D_{j'}^T(t')$ in this set, where $t' < t$, node j verifies its ZKP and extracts its associated loss. As a result, node j identifies K_V blocks with valid ZKPs that have the lowest loss values to form the parent block set $\mathcal{D}_j^V(t)$ for $D_j(t)$, with $|\mathcal{D}_j^V(t)| = K_V$. Then $D_j(t)$ is labeled as a tip block $D_j^T(t)$, and all tip blocks $D_{j'}^T(t') \in \mathcal{D}_j^V(t)$ are changed to unconfirmed status, i.e., $D_{j'}^U(t')$. Finally, $D_j^T(t)$ is integrated into the DAG by selecting the blocks in $\mathcal{D}_j^V(t)$ as its predecessors. As a result of these actions performed by all nodes, the AW values of the blocks on the DAG change, which may alter the validity status of some blocks. Specifically, certain blocks $D_{j''}^U(t'')$ for $t'' < t' < t$ become confirmed, i.e., they are updated to $D_{j''}^C(t'')$. Next, we explain how the AW of

each block on the DAG is altered and how the transition from tip to confirmed status occurs.

Fig. 1 illustrates a DAG ledger for two consecutive epochs $t-1$ and t . In epoch $t-1$, each vertex represents a block $D_{j_i}(t_i)$ by node j_i , for $i = 1, \dots, 4$, at epoch $t_i < t-1$. A direct edge from one vertex to another, for example, from $D_{j_2}^T(t_2)$ to $D_{j_1}^U(t_1)$, signifies that j_2 verifies block $D_{j_1}^U(t_1)$. Fig. 1 also displays the status evolution of the blocks after one epoch. A block is labeled as a tip if it lacks incoming validation edges. Therefore, in this figure, for epochs $t-1$ and t , the blocks $\{D_{j_2}^T(t_2), D_{j_3}^T(t_3), D_{j_4}^T(t_4)\}$ and $\{D_{j_5}^T(t_5), D_{j_6}^T(t_6)\}$ are tip blocks, respectively.

Moreover, a block that is neither a tip nor confirmed is referred to as an unconfirmed block. Hence, while blocks $\{D_{j_2}^T(t_2), D_{j_3}^T(t_3), D_{j_4}^T(t_4)\}$ are tips in epoch $t-1$, block $D_{j_3}^U(t_3)$ is classified as unconfirmed in epoch t , while $\{D_{j_2}^T(t_2), D_{j_4}^T(t_4)\}$ remain tips. Observe that the status of $D_{j_1}^U(t_1)$ transitions from unconfirmed to confirmed, which is denoted by $D_{j_1}^C(t_1)$. Specifically, a block achieves confirmed status when its AW surpasses a predefined threshold η . The AW is intricately linked to a weight vector that reflects the relative influence of the nodes.

The weight ω_j of each node j with $\omega_j > 0$ and $\sum_j \omega_j = 1$ is determined by the number of tokens it has staked. In DAG ledgers, staking refers to the process by which nodes lock their tokens to gain voting power in validating transactions and appending new blocks to the ledger. The more tokens a node stakes, the higher its associated validation weight, influencing the cumulative weight of the blocks it approves. This weight is assumed to remain constant over different epochs but can be dynamically adjusted based on node behavior. Specifically, if a node incorrectly disputes the validity of a block, as discussed in the challenge mechanism outlined in Sec. II-C, then a portion of its staked tokens is slashed as a penalty, directly reducing its weight ω_j . This incentivizes honest participation by making malicious behavior costly. To establish the network’s initial trust and ensure a secure starting point, a set of genesis blocks with confirmed status are proposed by the oracle committee (as discussed in Sec. III-B1) as trusted and correct blocks, providing a foundation for subsequent validations.

The AW of a block $D_{j_i}(t_i)$ is calculated as

$$\omega_{j_i} + \sum_{D_{j_{i'}}(t_{i'}) \in \mathcal{F}(D_{j_i}(t_i))} \omega_{j_{i'}},$$

where $\mathcal{F}(D_{j_i}(t_i))$ denotes the future cone of $D_{j_i}(t_i)$, encompassing all blocks that it validates, either directly or through a series of validations. For example, in Fig. 1 and in epoch t , blocks $\{D_{j_1}^C(t_1), D_{j_4}^U(t_4)\}$ are in the future cone of block $D_{j_6}^T(t_6)$, as block $D_{j_4}^U(t_4)$ is validated by it directly, while $D_{j_6}^T(t_6)$ validates block $D_{j_1}^C(t_1)$ indirectly. Moreover, Fig. 1 illustrates that the AW of block $D_{j_1}(t_1)$ surpasses η after the addition of the weights of blocks $D_{j_5}^T(t_5)$ and $D_{j_6}^T(t_6)$, and its status transitions from unconfirmed to confirmed.

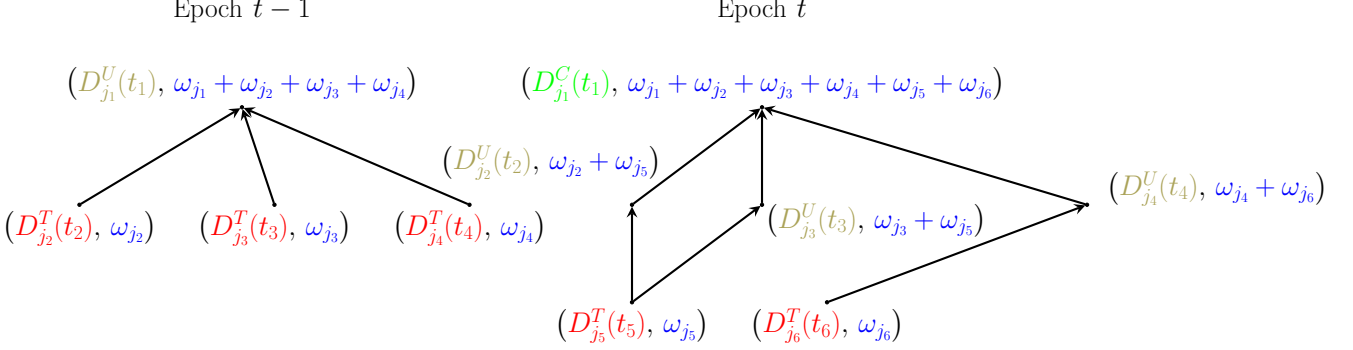


Fig. 1. Evolution of a DAG ledger over two consecutive epochs. Nodes are color-coded to indicate their status: red for tips, yellow for unconfirmed, and green for confirmed. The blue text represents the AW associated with each node.

C. Challenge Mechanism

In DAG ledgers, each block submission requires selecting parent blocks from the current set of tip blocks. Under normal circumstances, this process ensures that new blocks are seamlessly integrated into the network by referencing recent, valid blocks. However, a critical vulnerability known as the orphanage attack [37] exploits this mechanism. In an orphanage attack, malicious nodes intentionally select their own invalid blocks, or those of their colluding partners, as parents when submitting new blocks. By continuously referencing their own invalid blocks, these dishonest nodes effectively remove such blocks from the tip pool. Consequently, other honest nodes are unable to examine the validity of these blocks while selecting parents, allowing the invalidity of these strategically added blocks to go unnoticed. As a result, these invalid blocks remain hidden within the DAG despite being removed from the tip set. Later on, as the DAG grows, valid blocks may indirectly reference these previously isolated invalid blocks, causing them to accumulate weight over time. Ultimately, this process can lead to the confirmation of invalid blocks. The confirmation of such blocks not only compromises the quality of the global model derived from confirmed blocks but also alters the topology of the network, disrupting the integrity of the ledger.

The challenge mechanism is motivated by the need to counter this type of attack and restore transparency and fairness to the block selection process. This mechanism empowers honest nodes to flag and contest blocks that remain in an unconfirmed status within the DAG. The process begins with the detection of blocks impacted by an orphanage attack. At the core of this detection mechanism is graph reachability analysis (GRA) [38], [39], [40], a structural algorithm designed to identify blocks that have caused other blocks to become isolated within the DAG. The key principle behind GRA is that any valid block should be reachable from at least one tip block through a path in the DAG graph. If a block is found to be disconnected from all active tips, it indicates a potential issue: either the block was unintentionally abandoned due to network delays, or it was strategically isolated as part of an orphanage attack.

For each suspicious block identified through GRA,

the corresponding ZKP is verified. By definition, blocks involved in an orphanage attack are invalid, and their associated ZKPs will fail verification. Once such blocks are detected, the detecting node broadcasts a challenge to all trusted oracles within the network. Upon receiving a challenge, the oracles compile a list of disputed blocks and independently verify their validity based on the provided ZKPs.

Following verification, the oracles participate in a supermajority voting process: if more than 2/3 of the oracles agree that a block is invalid, it is formally revoked from the DAG. Block revocation means that the invalid block is excluded from future parent selections, and the AW of affected blocks is updated accordingly to neutralize the impact of the revoked block on the network. Conversely, if a supermajority of oracles determine that the disputed block is valid, the network penalizes the challenging node j by slashing a fraction of its tokens. This penalty reduces the challenger's ω_j , thereby decreasing its influence and voting power within the DAG for future block submissions. Remark II.3. While an incorrect dispute results in penalizing the disputing node, ZK-HybridFL does not penalize the submitter of an invalid block. This design choice reflects a balance between encouraging participation and acknowledging that honest mistakes or network delays can lead to inadvertent errors. Penalizing such actions could stifle honest contributions, especially when no malicious intent is involved. In contrast, initiating a challenge, especially one that incorrectly disputes a valid block, incurs significant costs by triggering a consensus process among oracles and resulting in computational overhead.

III. EDSC Mechanism of ZK-HybridFL

Our proposed ZK-HybridFL system employs event-driven smart contracts (EDSCs) to automate predefined actions in response to specific network events. By routing every off-chain emission through a single EventAdmission contract (backed by the OracleRegistry), we avoid constant polling and heavyweight sidechain consensus while ensuring that only vetted, canonical events can trigger on-chain logic. Sec. III-A details the main EDSCs used in ZK-HybridFL, and Sec. III-B1 describes the Oracle Committee's verification and event-publication process.

In ZK-HybridFL, all EDSCs are deployed on a dedicated sidechain that isolates contract execution from the main ledger. This design boosts throughput and scalability by handling high-frequency interactions off-chain, without burdening the primary network. The sidechain architecture and its integration within the broader protocol are presented in Sec. S2-A2. A more detailed technical description of the Oracle Committee and the sidechain's event-ordering mechanism is available in the supplementary material (Sec. S2).

A. Smart Contracts in ZK-HybridFL

Each node j in the ZK-HybridFL process deploys five EDSCs $\{S_j^k\}_{k=1}^5$ on the sidechain, which are independently triggered by validated events from the oracle. Next, we delineate the function and process of each of these five EDSCs.

1) Validation Smart Contract S_j^1 : S_j^1 validates the ZKP bundles of the blocks in $\mathcal{D}_j^T(t)$. It subscribes to the EventApproved log emitted by the EventAdmission contract (cf. Sec. S2-A1), which the Oracle Committee emits once it has vetted node j' 's DAG-published bundle $Z_{j'}^{t'}$. For each block $D_{j'}^{T'}(t') \in \mathcal{D}_j^T(t)$, S_j^1 retrieves from the sidechain the commitments

$$C_{j'}^{t', \text{model}}, \quad C_{j'}^{t', \text{test}},$$

and the global verification key vk . It then fetches $\Pi_{j'}^{t'}$, $\mathcal{Y}_{j'}^{t'}$, and $\mathcal{L}_{j'}^{t'}$ from the bundle $Z_{j'}^{t'}$ on the DAG, invokes

$$\text{Verify}(\text{vk}, \Pi_{j'}^{t'}, C_{j'}^{t', \text{model}}, C_{j'}^{t', \text{test}}, \mathcal{Y}_{j'}^{t'}, \mathcal{L}_{j'}^{t'}),$$

and retains the block only if the call returns 1. After processing all candidates, S_j^1 ranks the verified blocks by their loss values $\mathcal{L}_{j'}^{t'}$ and selects the top K_V with the lowest loss to form $\mathcal{D}_j^V(t)$. This finalizes the contract's state, enabling node j to adopt these blocks as parents in the next stage of ZK-HybridFL.

2) Submission Smart Contract S_j^2 : S_j^2 facilitates the submission of node j 's new block $D_j(t)$ to the DAG and updates the aggregated weight (AW) of existing blocks. It subscribes to the EventApproved log emitted by the EventAdmission contract (cf. Sec. S2-A1), which is triggered once the Oracle Committee has vetted and approved the validated set $\mathcal{D}_j^V(t)$. The event communicates that node j has determined the parent blocks from $\mathcal{D}_j^V(t)$ for its new block $D_j(t)$; it includes necessary information on these parent blocks alongside the model update \mathbf{W}_j^t and corresponding ZKP Z_j^t contained in $D_j(t)$. S_j^2 then updates the AW values associated with the vertices corresponding to these blocks within $\mathcal{D}_j^V(t)$ on the DAG and their ancestors, acknowledging their role as parents of the new block. Following this update, S_j^2 labels $D_j(t)$ as a new tip of the DAG (denoted $D_j^T(t)$), while altering the status of each parent block $D_{j'}^{T'}(t') \in \mathcal{D}_j^V(t)$ from tip to unconfirmed (denoted $D_{j'}^U(t')$). If the updated AW of any block exceeds a predetermined threshold, S_j^2 marks such blocks as confirmed. In its final step, S_j^2

transitions its state to complete by embedding $D_j^T(t)$ into the DAG as a new vertex. This vertex is connected via directed edges to the vertices corresponding to the parent blocks in $\mathcal{D}_j^V(t)$, effectively updating the DAG structure to reflect the addition of node j 's block and the revised parent relationships.

3) Challenge Smart Contract S_j^3 : S_j^3 manages the dispute mechanism for potentially invalid blocks within the ZK-HybridFL framework. It subscribes to the EventApproved log emitted by the EventAdmission contract (cf. Sec. S2-A1), which the Oracle Committee emits once it has vetted node j 's off-chain graph reachability analysis (GRA) detection of a suspicious block $D_{j'}(t')$. Upon triggering, S_j^3 receives the GRA detection results as inputs comprising the identifiers of the suspicious blocks $\{D_{j'}(t')\}$, the identity of the node j' that created them, relevant ZKPs or metadata supporting the suspicion, and a fraction of node j 's tokens staked as collateral.

Following receipt of these inputs, S_j^3 notifies trusted oracles of the questionable blocks by emitting an event containing details of the suspicious blocks, GRA findings, and supporting evidence. Simultaneously, the contract holds the staked tokens in escrow. This notification prompts the oracles to validate the challenge: they assess the evidence to determine the validity of the suspicious blocks. The output of S_j^3 thus involves alerting the oracles and securely holding the stake while awaiting their consensus. Depending on the oracles' decision, S_j^3 then updates its state accordingly. If the oracles confirm that the challenged blocks are invalid, S_j^3 marks these blocks as revoked within the DAG ledger, ensuring the integrity of the ledger by potentially reconnecting or adjusting references as needed, and releases the staked tokens back to node j . Conversely, if the oracles find the challenge unfounded, S_j^3 imposes a penalty by slashing the staked tokens, reducing node j 's future influence, and maintains the status of the challenged blocks. This final state transition solidifies the resolution of the dispute, either by cleansing the DAG of invalid blocks or by penalizing incorrect challenges.

4) Model Aggregator Smart Contract S_j^4 : S_j^4 is assigned to compute the global model $\tilde{\mathbf{W}}_j^t$ for node j . It subscribes to the EventApproved log emitted by the EventAdmission contract (cf. Sec. S2-A1), which the Oracle Committee emits once node j has signaled availability for epoch $t+1$ and the dispute resolution in S_j^3 has concluded. This event carries the latest AW of DAG blocks along with their updated validity status. Upon receiving that log, S_j^4 determines the set \mathcal{J}_j^t of all nodes j' that produced at least one new confirmed block in epoch t . For each j' , it identifies the most recent epoch $t_{j'}^*$, such that $D_{j'}^{t_{j'}^*}$ became confirmed in epoch t , and retrieves the corresponding model update $\mathbf{W}_{j'}^{t_{j'}^*}$. The contract then computes the global model via weighted aggregation:

$$\tilde{\mathbf{W}}_j^t = \sum_{j' \in \mathcal{J}_j^t} \frac{\omega_{j'}}{\sum_{k \in \mathcal{J}_j^t} \omega_k} \mathbf{W}_{j'}^{t_{j'}^*},$$

TABLE I
Summary of EDSCs for ZK-HybridFL.

SC	Major Defined Event Subscription	Input	Output	State
S_j^1	Generation of ZKP Z_j^t	Triggers validation of proofs Z_j^t in blocks $D_j^T(t')$	Validation results of ZKPs and performance evaluations, forming set $\mathcal{D}_j^V(t)$	Transition to complete after sending results to node j
S_j^2	Formation of set $\mathcal{D}_j^V(t)$	Identifies and verifies valid blocks within $\mathcal{D}_j^V(t)$ on the DAG	Updates DAG by labeling block $D_j(t)$ as tip $D_j^T(t)$, changes status of parent blocks	Releases contributed block $D_j^T(t)$ into the DAG
S_j^3	Detection of potentially invalid block $D_j(t')$	Receives GRA detection results and token stake from node j , including flagged blocks $\{D_j(t')\}$ and relevant ZKPs	Notifies oracles of suspicious blocks and stakes tokens in escrow; oracles verify challenge validity and determine slashing or refund	Updates DAG by marking invalid blocks and slashing tokens if the challenge fails; returns tokens if challenge succeeds
S_j^4	Announcement of trainer availability for next epoch $t + 1$	Aggregates model updates $\mathbf{W}_j^{t'}$ from confirmed blocks $D_j^C(t')$	Generates global model $\tilde{\mathbf{W}}_j^t$ for epoch $t + 1$ via aggregation rule	Sends global model $\tilde{\mathbf{W}}_j^t$ to node j
S_j^5	Formation of block $D_j^T(t)$	Verifies completion and integration of model update $D_j^T(t)$ and model \mathbf{W}_j^t	Determines reward amount based on predefined criteria (e.g., accuracy, contribution quality)	Releases calculated reward to trainer node j via blockchain transaction

ensuring that only the latest confirmed update from each node contributes and that weights are normalized over \mathcal{J}_j^t . Once aggregation completes, S_j^4 transitions to the complete state and returns $\tilde{\mathbf{W}}_j^t$ to node j , enabling it to commence the next training epoch. A detailed ablation study validating the benefits of this stake-weighted aggregation scheme over uniform averaging is presented in the supplementary material (Sec. S3-C1).

5) Reward Distribution Smart Contract S_j^5 : S_j^5 is allocated for dispensing rewards to trainer node j upon successful submission of its contributed block $D_j^T(t)$. It subscribes to the EventApproved log emitted by the EventAdmission contract (cf. Sec. S2-A1), which the Oracle Committee emits once the submission process in S_j^2 has concluded. This event provides information regarding the contributed block $D_j^T(t)$, its corresponding model \mathbf{W}_j^t , and the verification details confirming successful integration into the DAG. Specifically, once triggered, S_j^5 verifies the final status of block $D_j^T(t)$ and the correctness of \mathbf{W}_j^t , as endorsed by the oracle. It then calculates the reward amount based on established criteria such as model accuracy and the number of valid blocks that node j has successfully introduced into the system. After finalizing the reward, S_j^5 transitions its state to complete by creating a transaction on the sidechain to credit the trainer node j 's account with the calculated sum.

Table I summarizes the structure of the smart contracts for ZK-HybridFL, where the input, output, and state variables of these EDSCs in epoch t are denoted as $\{I_j^k(t), O_j^k(t), P_j^k(t)\}_{k=1}^5$.

B. Oracle-assisted Sidechain

1) Oracle Committee: In ZK-HybridFL, the Oracle Committee acts as a trusted intermediary responsible for verifying events published by the nodes before they trigger the EDSCs. When a node publishes an event intended to trigger a smart contract, the oracles initially place a hold on the event and verify it to ensure that it adheres to the expected structure and contains accurate information. For instance, the Oracle Committee checks that the event's content is consistent with the data recorded on the DAG

ledger, such as the associated ZKPs, and that the performance metrics in the event align with the corresponding blocks in the DAG. If the event passes all verification checks, the oracles lift the hold on the event within the sidechain, allowing it to trigger any subscribed smart contracts. This process ensures that the event is neither malicious nor incorrectly formatted, thereby preventing invalid events from triggering smart contracts.

This verification mechanism is critical in ZK-HybridFL because, unlike conventional sidechains that use dedicated consensus protocols such as Raft in ChainFL, our sidechain does not employ a separate consensus process. Instead, the Oracle Committee acts as a lightweight verification layer, reducing the overhead typically associated with consensus protocols while ensuring that only valid events can trigger smart contracts. This approach minimizes the scalability limitations of the sidechain by offloading event validation to the Oracle Committee, allowing the DAG ledger to remain the primary consensus layer without bottlenecks caused by sidechain consensus.

2) Sidechain: The ZK-HybridFL sidechain serves as a specialized ledger for storing and executing EDSCs, ensuring that high-frequency interactions do not overload the DAG. Its block structure is designed to encapsulate the data elements essential for the protocol's operation and network logistics. In the initial blocks, the sidechain records identifiers that distinguish oracle nodes—responsible for validating events—from non-oracle participants, along with stake-related metadata that determines each node's weight ω_j . During the network's one-time deployment phase, EDSCs are deployed on the sidechain. Once live, subsequent blocks record interactions with these EDSCs, capturing dynamic information such as commitments $H(\mathcal{D}_j^{t,\text{test}})$ and $H(\mathbf{W}_j^t)$, proof verifiers v_j^t for each node j and epoch t , reward distributions for successful model submissions, and updates to tokens staked by participants.

Unlike conventional blockchains that rely on consensus mechanisms such as proof of work (PoW) to validate blocks, the ZK-HybridFL sidechain adopts a different strategy. In traditional blockchains, consensus is used to ensure all nodes agree on a single, unique sequence of

blocks. For example, in PoW-based systems, nodes compete to propose the next block by solving a computational puzzle. Once a node successfully proposes a block, the network agrees to attach that block to the chain, establishing transaction order and conflict resolution. Consequently, any transaction included in an earlier block (e.g., Block A) is recognized as having occurred before transactions in subsequently attached blocks (e.g., Block B).

In contrast, the ZK-HybridFL sidechain does not use a separate consensus algorithm for block validation. Instead, it leverages its event-driven architecture to inherently maintain transaction order. When an event is validated and a corresponding block is attached to the sidechain, the timestamp of this attachment determines the transaction order. Thus, if a transaction is included in a block that is attached with an earlier timestamp, it is automatically considered to have occurred before transactions in later-attached blocks. This built-in ordering mechanism eliminates the need for additional consensus protocols, simplifying transaction validation and ordering on the sidechain.

In decentralized networks like ZK-HybridFL, relying on a single global clock such as a real-world timestamp introduces significant challenges [41]. Clock drift, network latency, and the absence of a trusted time authority all make it difficult to maintain an accurate and uniform notion of time across all nodes. Consequently, event ordering becomes prone to inconsistencies and disagreements when purely dependent on physical clocks. To address this, ZK-HybridFL adopts Lamport clocks [42], which assign logical timestamps reflecting the causal dependencies among events, rather than relying on physical time references. By doing so, the system circumvents the complexities of clock synchronization in a heterogeneous environment while still guaranteeing a deterministic and consistent event sequence. As each oracle increments its local counter and exchanges logical timestamps with peers, a coherent final order naturally emerges even under asynchronous conditions. This ensures conflict-free execution of smart contracts and recording their corresponding events on the sidechain and allows all nodes to reconcile their states without resorting to traditional consensus protocols. For more details about ordering events in a decentralized network using Lamport clocks, the reader can refer to [43].

IV. The ZK-HybridFL Procedure and Analysis

A. Workflow of ZK-HybridFL

This subsection outlines the workflow of ZK-HybridFL from the viewpoint of node j at epoch t . It describes how node j performs local training, commits its state, generates proofs, submits blocks, and participates in the on-chain verification, challenge, and aggregation stages.² These four stages repeat until the model converges.

²All on-chain triggers in Stages 2–4 result from threshold-signed EventApproved logs emitted by the EventAdmission contract. These logs are produced only after off-chain validation by the Oracle Committee; see Sec. S2-A1.

1) Stage 1: Training and Proof Certification:

- Local training. Node j downloads the latest global model \mathbf{W}_j^{t-1} from the sidechain and runs R stochastic gradient descent (SGD) iterations on its private training batch $\mathcal{D}_j^{t,\text{train}}$ (mini-batch size B), yielding updated weights \mathbf{W}_j^t .
- Commit. It posts two KZG commitments

$$C_j^{t,\text{model}} = \text{Commit}(\mathbf{W}_j^t), \quad C_j^{t,\text{test}} = \text{Commit}(\mathcal{D}_j^{t,\text{test}})$$

to the sidechain, together with a Lamport timestamp.

- Proof generation (off-chain). Using the universal proving key pk , node j evaluates the inference circuit on its private witness $(\mathbf{W}_j^t, \mathcal{D}_j^{t,\text{test}})$ and produces the noninteractive Groth16 proof Π_j^t . It then assembles the proof bundle

$$Z_j^t = (\Pi_j^t, \mathcal{Y}_j^t, \mathcal{L}_j^t, C_j^{t,\text{model}}, C_j^{t,\text{test}})$$

and buffers it locally until submission.

- Block construction. Once Π_j^t is ready, node j forms the block

$$D_j(t) = [\mathbf{W}_j^t, Z_j^t]$$

for insertion into the DAG.

2) Stage 2: Block Submission:

- Fetch tips. Node j reads the latest approved events to reconstruct the current tip set $\mathcal{D}_j^T(t)$ and pulls each tip's commitments $C_{j'}^{t',\text{model}}$, $C_{j'}^{t',\text{test}}$ and the global verification key vk from the sidechain.
- Verification. Node j invokes the validation smart contract S_j^1 , which, for each candidate block, performs

$$\text{Verify}(\text{vk}, \Pi_{j'}^{t'}, C_{j'}^{t',\text{model}}, C_{j'}^{t',\text{test}}, \mathcal{Y}_{j'}^{t'}, \mathcal{L}_{j'}^{t'})$$

and returns the top- K_V verified parents $\mathcal{D}_j^V(t)$.

- Publish block. With $\mathcal{D}_j^V(t)$ confirmed, node j calls S_j^2 , which (i) records the chosen parents, (ii) embeds $D_j(t)$ into the DAG, and (iii) marks it as a new tip.

3) Stage 3: Consensus-Driven Confirmation and Challenge:

- Node j syncs with the sidechain, incorporating new blocks $D_{j'}(t)$ whose approved events have appeared on chain.
- Upon synchronization, S_j^2 advances to its second phase: it updates block statuses and records which blocks transition from unconfirmed to confirmed in epoch t .
- Node j executes graph reachability analysis (GRA) on the DAG.
- Based on the GRA output, node j may trigger the challenge contract S_j^3 to dispute the validity of certain blocks.
- If triggered, S_j^3 stakes tokens from node j and notifies the oracles to adjudicate the dispute.
- Depending on the oracles' consensus (cf. Sec. II-C), either the DAG is updated or node j 's stake is slashed.

4) Stage 4: Global Model Aggregation:

- Node j calls the aggregation smart contract S_j^4 with the list of confirmed blocks from epoch t .
- S_j^4 retrieves the corresponding models from the DAG and computes the new global model $\tilde{\mathbf{W}}_j^t$, storing it on the sidechain.
- Finally, node j invokes the reward contract S_j^5 , which disburses tokens to node j based on its contributed loss \mathcal{L}_j^t (cf. Sec. III-A5).

At this point, node j holds the updated global model $\tilde{\mathbf{W}}_j^t$ and begins the next epoch's local training, returning to Stage 1.

Remark IV.1. The four-stage protocol in Sec. IV-A remains intact; we simply augment Stages 1 and 2 to consume the committee-published scalars $[L_t, B_t]$ and τ_{\max} . At the boundary between epochs $t - 1$ and t , each node j retrieves the signed events `NormThresholdsPublished` and `CosineThresholdsPublished` (see Sec. S2-B1) and caches the new bounds before beginning Stage 1. After local training and KZG commitments, Stage 1 proof generation now emits three noninteractive proofs: Π_j^t (Groth16 for correct inference and loss), Σ_j^t (Bulletproof enforcing $L_t \leq \|\Delta \mathbf{W}_j^t\|_2 \leq B_t$), and Γ_j^t (Groth16 subproof enforcing $\cos(z_{\text{old}}, z_{\text{new}}) \leq \tau_{\max}$ on the fixed probe set). These are concatenated into the extended bundle $Z_j^{t,\text{ext}}$. Stage 2's validation contract S_j^1 then runs the three-step verification (Groth16 Π_j^t , Bulletproof Σ_j^t , cosine subproof Γ_j^t) as in Sec. S2-B2 and returns the top- K_V parents exactly as before. Stages 3 and 4 continue to react only to the usual `ProofOK` events and require no modifications.

Remark IV.2. In ZK-HybridFL, the network can be effectively divided into two types of nodes—full nodes and light nodes—based on their resource capabilities. This division is motivated by the need to accommodate diverse participant environments, optimize system performance, and ensure scalability. Full nodes, with ample computational power and storage, maintain the complete global DAG ledger, comprehensive sidechains, and carry out resource-intensive tasks, including oracle functions. These nodes handle heavy operations such as ledger maintenance, smart contract execution, and dynamic event validation, which are crucial for the integrity and reliability of the overall system.

In contrast, light nodes operate with lighter versions of the DAG and sidechain, focusing on essential local training and basic participation in the FL process. By delegating complex, resource-heavy tasks to full nodes, light nodes can efficiently contribute to model updates and generate proofs without the burden of maintaining an entire global state. This stratification not only leverages the strengths of more capable participants but also enables a wide range of devices with limited resources to join the network. The oracle functionality, consistent across both node types, serves as a trusted intermediary, validating events and bridging interactions between light and full nodes. Fig. 2 illustrates the architectural division between full nodes and light nodes in ZK-HybridFL. The overall interaction



Fig. 2. Full nodes (FNs) maintain a complete DAG (FN_DAG) and sidechain (FN_SC) while handling oracle functions. Light nodes (LNs) use a trimmed DAG (LN_DAG) and lightweight sidechain (LN_SC), with LN_M serving as the LN's core controlling module.

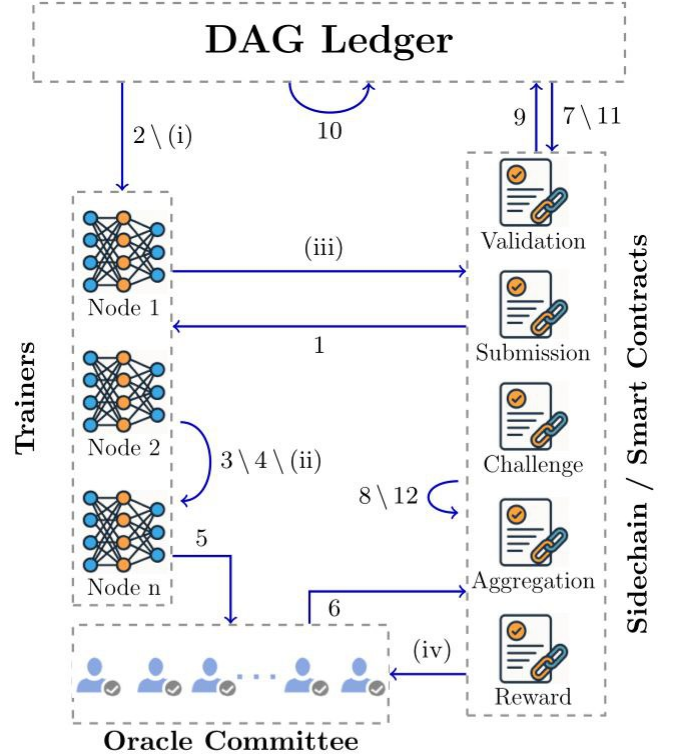


Fig. 3. ZK-HybridFL workflow (1–12): 1) aggregate IDs; 2) fetch blocks; 3) local train; 4) bundle proofs; 5) submit bundle; 6) committee admit; 7) fetch ZKP tips; 8) validate ZKPs; 9) parent selection; 10) attach block; 11) update weights; 12) aggregate and reward. Challenge loop (i–iv): (i) fetch proof; (ii) local GRA; (iii) submit proof; (iv) reward or slash.

between the trainers, the Oracle Committee, the sidechain smart contracts, and the DAG ledger is illustrated in Fig. 3, including both the main training and challenge phases.

V. Simulation Results

In this section, we describe the simulation setup and present experimental results comparing ZK-HybridFL with Blade-FL and ChainFL. A comprehensive analysis between ZK-HybridFL and ChainFL from both learning and distributed-ledger perspectives is provided in the supplementary material (Sec. S3-A).

A. Simulation Setup

To simulate Blade-FL and ChainFL, we use their public implementations from the respective GitHub repositories [44], [45], with minor modifications to match our

experimental protocol. For ZK-HybridFL, the federated learning (FL) process is built using TensorFlow Federated (TFF) [46] to simulate local model training across distributed nodes. Training with a mini-batch of size B consists of R stochastic gradient descent (SGD) iterations per FL epoch, inducing heterogeneous compute loads across nodes.

For decentralized coordination, the blockchain architecture integrates a directed acyclic graph (DAG) ledger, simulated using the GoShimmer framework [47], to manage parallelized model-update submissions. A Substrate-based sidechain [48] hosts the core smart contracts (cf. Sec. III) for ZKP verification, model aggregation, challenge resolution, and reward distribution. WebAssembly (Wasm)-based [49] contracts ensure low-overhead execution of this logic. DAG-sidechain communication is implemented via gRPC [50], and Apache Kafka [51] serves as a message broker for the event-driven architecture. ZKPs are generated using EZKL [52] and zkML [53].

We denote n as the total number of nodes, γ as the percentage of lazy nodes, and μ as the percentage of adversarial nodes. The corresponding counts are $\lfloor n\gamma \rfloor$ and $\lfloor n\mu \rfloor$, respectively, where $\lfloor \cdot \rfloor$ denotes rounding. Lazy nodes in all three schemes simply resubmit a model update from one or more past epochs instead of retraining.

Adversarial nodes are modeled as follows. In Blade-FL, the adversarial set collectively controls 51% of the proof-of-work (PoW) hashing power, dominating block creation and ensuring that their noisy updates are predominantly used in global aggregation. The parameter μ controls how many nodes are adversarial, but the group as a whole always holds 51% of the hash power. Thus, smaller μ yields fewer but more powerful adversarial nodes, whereas larger μ spreads the same total PoW across more attackers. In ChainFL and ZK-HybridFL, adversaries (i) add structured noise to their locally trained updates and (ii) conduct orphanage attacks by repeatedly selecting their own or colluding blocks as parents in the DAG, thereby boosting the aggregated weight of adversarial blocks.

Unless otherwise stated, the mini-batch size is $B = 50$, the number of local SGD iterations per epoch is $R = 5$ with learning rate $\eta = 0.01$, and each submitted block in ZK-HybridFL selects $K_V = 4$ parent blocks.

To emulate realistic network conditions, nodes are assigned heterogeneous bandwidths in the range 10 Mbps–50 Mbps and latencies in the range 50 ms–200 ms. These parameters are intrinsic inputs to the simulator and are chosen to reflect typical wide-area settings.

B. Learning Tasks

Task 1: Image Classification

Task 1 uses the MNIST dataset with 70,000 grayscale images of size 28×28 across ten classes (digits 0–9). A lightweight convolutional neural network (CNN) based on MobileNetV2 [54] is used. The evaluation metric is classification accuracy, i.e., the fraction of correctly classified test samples.

For Blade-FL and ChainFL, 10,000 images are reserved as a public validation dataset, and the remaining 60,000 images are evenly distributed among the n nodes. Each node splits its local data into 80% for training and 20% for testing. In ZK-HybridFL, there is no public validation dataset; instead, all 70,000 images are evenly split across nodes, again with an 80%–20% train–test split, and 20% of each node’s local test data is further designated as a private inference batch for ZKP generation. All reported test accuracies are computed on the aggregated local test sets of each scheme; the public datasets (Blade-FL, ChainFL) and private inference batches (ZK-HybridFL) are used only for validation, not for final evaluation.

Task 2: Text Sentiment Analysis

Task 2 is a next-word prediction task using a gated recurrent unit (GRU)-based language model trained on the Penn Treebank dataset with 345,526 tokens. The model outputs a probability distribution over the vocabulary for each next word. Performance is evaluated via perplexity,

$$\text{Perplexity} = \exp\left(-\frac{1}{N} \sum_{i=1}^N \log p_{y_i}\right),$$

where p_{y_i} is the predicted probability of the true next word y_i at position i , and N is the total number of predictions. Lower perplexity indicates better predictions.

For Blade-FL and ChainFL, 45,526 tokens are reserved as a public validation dataset, and the remaining 300,000 tokens are evenly distributed among the n nodes. Each node uses 80% of its tokens for local training and 20% for local testing. In ZK-HybridFL, each node additionally marks 20% of its local test subset as a private inference batch for ZKP generation.

C. Results and Analysis

1) Learning Perspectives:

FL training convergence: Fig. 4 shows the training-loss trajectories of Blade-FL, ChainFL, and ZK-HybridFL in a network with $n = 15$ nodes, $\mu = 20\%$ adversarial nodes, and $\gamma = 10\%$ lazy nodes. Blade-FL achieves moderate loss reduction in early epochs but ultimately fails to converge. Once adversarial nodes effectively control 51% of the PoW computation, they dominate block creation, and their noisy updates increasingly contaminate the global model, preventing convergence to a low-loss solution.

ChainFL converges better than Blade-FL due to its DAG-based and sharded design. However, it remains inferior to ZK-HybridFL. As discussed from the ledger perspective in Sec. S3-A2, ChainFL’s dependence on a public reference dataset for validation makes it vulnerable to lazy nodes that resubmit stale updates which still pass the validation threshold. Furthermore, adversarial nodes can influence tip-based selection on the DAG and introduce subtle corruptions into the global model, preventing convergence to very low loss.

ZK-HybridFL, by contrast, leverages ZKPs and a loss-aware DAG policy (cf. Sec. II-B) to ensure that only

freshly trained, correctly validated updates contribute to aggregation. Even in the presence of adversarial and lazy behavior, invalid or stale updates are systematically filtered. This is reflected in the consistently decreasing loss curve of ZK-HybridFL, which indicates steady progress toward a high-quality model.

Invalid model detection: Fig. 5 reports the number of invalid models detected over time for the same setting as Fig. 4. A model is considered invalid if it fails to satisfy the scheme-specific inclusion criteria for global aggregation. In Blade-FL, an update is invalid if, after being broadcast and signed, it is never included in a mined block. In ChainFL, an update is invalid if it is not selected as a DAG parent within a prescribed staleness window, rendering it permanently ineligible for future parent selection. In ZK-HybridFL, a model is invalid if it is revoked via the challenge mechanism (cf. Sec. II-C).

The horizontal reference line in Fig. 5 corresponds to an ideal system that perfectly detects all invalid models. Blade-FL performs worst: many invalid updates remain undetected or are detected late. ChainFL performs better but still lags significantly behind ZK-HybridFL.

ZK-HybridFL initially flags fewer invalid models than the other two schemes, because a formal revocation requires completion of the challenge procedure and oracle adjudication. Thus, a model may be added in one epoch and only revoked several epochs later. Over time, however, ZK-HybridFL “catches up,” and the cumulative number of revoked models approaches the ideal line. Combined with Fig. 4, this behavior confirms the learning-theoretic analysis in Sec. S3-A1: by ensuring that only valid, high-quality updates influence the global model, ZK-HybridFL achieves both faster convergence and stronger robustness in the presence of adversarial and lazy nodes.

Model performance vs. number of nodes: Fig. 6 plots test accuracy (Task 1) and perplexity (Task 2) as the number of nodes n ranges from 5 to 30, with $\mu = \gamma = 15\%$ fixed. For Task 1, ZK-HybridFL rapidly improves from accuracy 0.80 at $n = 5$ to 0.90 at $n = 10$ and 0.95 at $n = 15$, then saturates near 0.98–0.99 for $n \geq 20$. This steep improvement demonstrates that the ZKP-gated validation pipeline successfully exploits larger networks: additional honest nodes yield more high-quality updates, while adversarial and lazy contributions are suppressed.

ChainFL’s accuracy increases more slowly, from 0.55 at $n = 5$ to 0.70 at $n = 30$. Its architecture partially dilutes malicious contributions, but the use of a public dataset for validation still allows stale or subtly corrupted updates to pass the threshold, limiting the benefits of larger network sizes.

Blade-FL suffers as the network grows: accuracy starts at 0.45 with 5 nodes and drops to 0.33 at 30 nodes, highlighting the fragility of PoW-based consensus under adversarial conditions.

Task 2 exhibits an analogous pattern. ZK-HybridFL consistently achieves the lowest perplexity, decreasing from 145.73 at $n = 5$ to 117.67 at $n = 30$. ChainFL improves from 218.59 to 167.08 over the same range, while

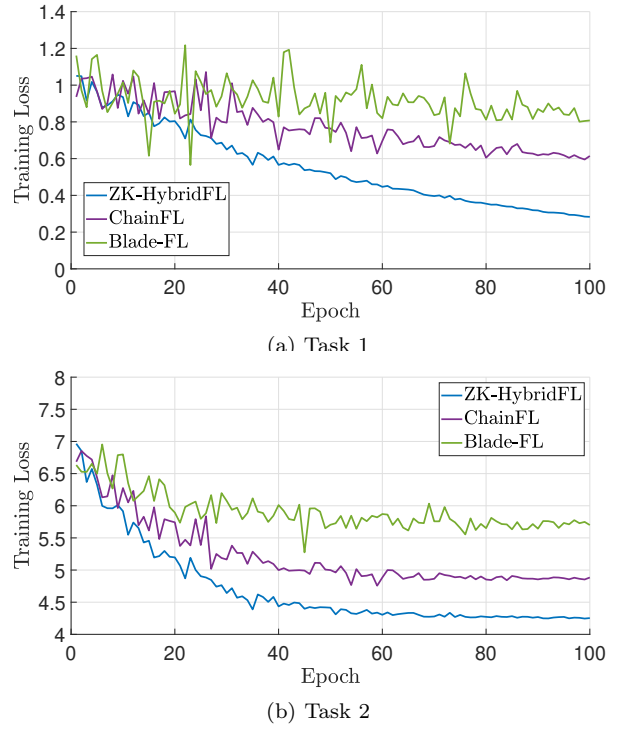


Fig. 4. Training loss of Blade-FL, ChainFL, and ZK-HybridFL for $n = 15$, $\mu = 20\%$ adversaries, $\gamma = 10\%$ lazy nodes, $R = 5$, and $B = 50$.

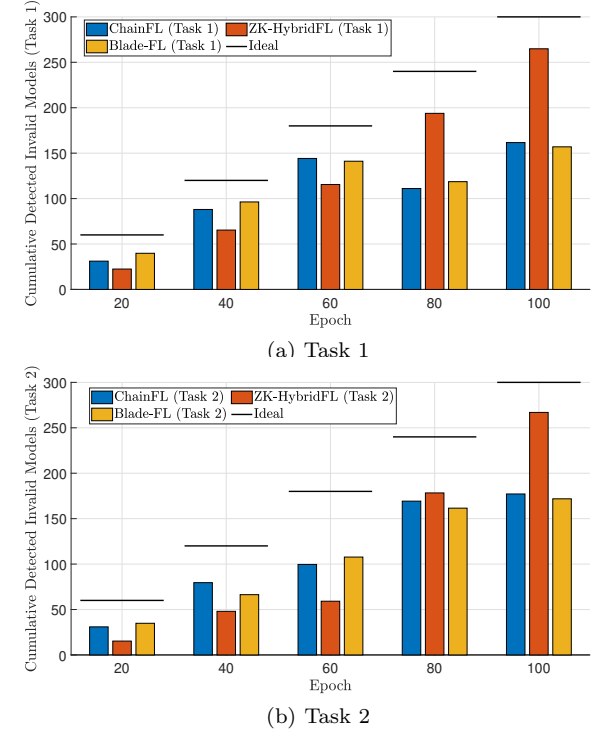
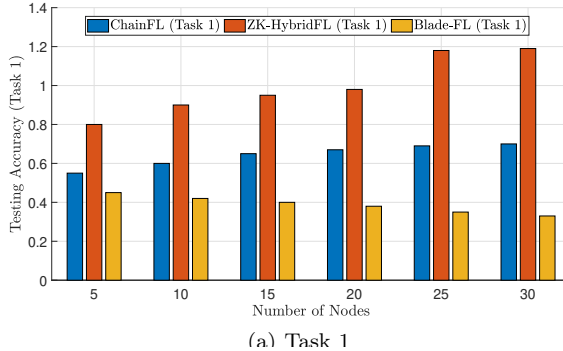
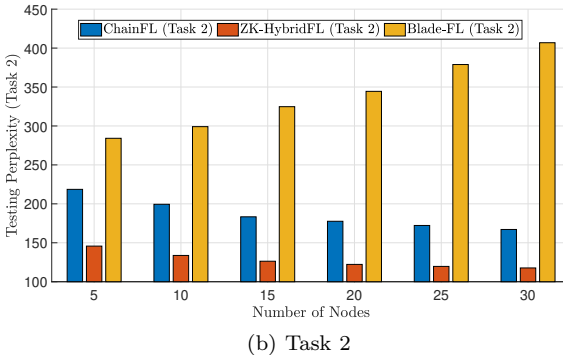


Fig. 5. Number of detected invalid models over training epochs, corresponding to Fig. 4.

Blade-FL degrades from 284.17 to 406.89. These results reinforce that only ZK-HybridFL fully capitalizes on larger networks by ensuring that the additional capacity is translated into higher-quality, validated updates.



(a) Task 1



(b) Task 2

Fig. 6. Model performance versus number of nodes n for ZK-HybridFL, ChainFL, and Blade-FL with $\mu = \gamma = 15\%$.

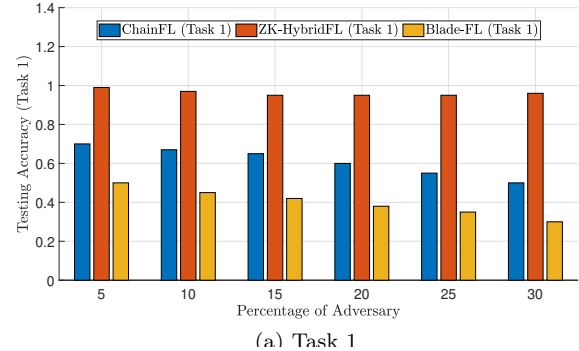
Model performance vs. percentage of adversarial nodes: Fig. 7 shows test accuracy (Task 1) and perplexity (Task 2) as the adversarial ratio μ increases from 5% to 30%, with $n = 15$ and $\gamma = 15\%$ fixed. For Task 1, ChainFL’s accuracy drops from 0.70 at $\mu = 5\%$ to 0.50 at $\mu = 30\%$, reflecting its vulnerability to adversaries that exploit the public validation dataset and tip-based aggregation. Blade-FL starts at 0.50 and degrades sharply to 0.30, highlighting the susceptibility of PoW-based consensus to majority-hash attacks.

ZK-HybridFL exhibits strong robustness, maintaining accuracy near 0.99 at $\mu = 5\%$ and still achieving 0.88 at $\mu = 30\%$. The ZKP-gated inference validation and loss-aware DAG aggregation jointly prevent adversarial nodes from quietly introducing corrupted updates into the global model.

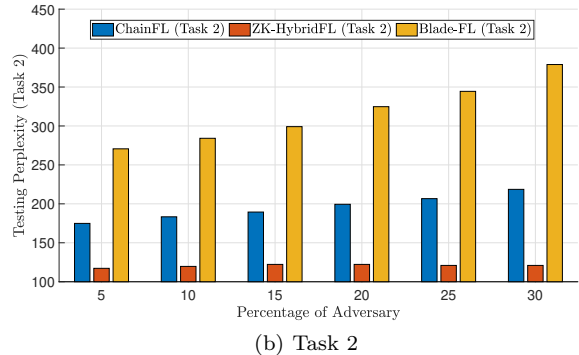
For Task 2, the same qualitative trends hold. ZK-HybridFL retains low perplexity, increasing only from 117.18 to 120.92 as μ grows from 5% to 30%. ChainFL’s perplexity worsens from 174.87 to 218.59, and Blade-FL’s from 270.64 to 378.89. These results underscore the benefit of ZK-HybridFL’s dual-layer validation over the mechanisms employed in Blade-FL and ChainFL.

Model performance vs. percentage of lazy nodes: Fig. 8 reports test accuracy (Task 1) and perplexity (Task 2) as the lazy-node ratio γ increases from 5% to 30%, with $n = 15$ and $\mu = 15\%$ fixed. Lazy nodes resubmit past models without retraining, polluting aggregation with stale information.

For Task 1, ChainFL’s accuracy decreases from 0.73 to 0.60, and Blade-FL’s from 0.55 to 0.42, as γ increases. ZK-HybridFL remains highly accurate, dropping only from



(a) Task 1



(b) Task 2

Fig. 7. Model performance versus adversarial ratio μ for ZK-HybridFL, ChainFL, and Blade-FL with $n = 15$ and $\gamma = 15\%$.

0.99 to 0.94, owing to its ability to detect and discard stale updates.

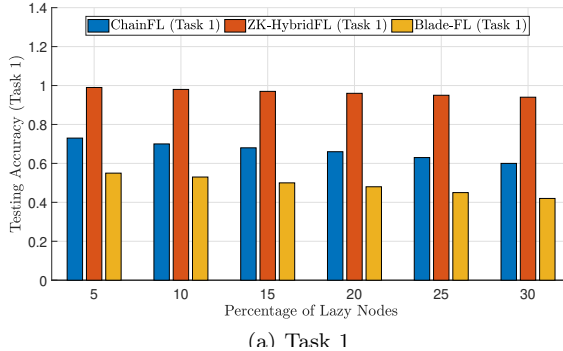
For Task 2, ChainFL’s perplexity increases from 169.65 to 199.42 as γ grows, since stale submissions can still satisfy the public validation threshold. Blade-FL, already stressed by adversarial behavior, degrades from 241.85 to 307.21. In contrast, ZK-HybridFL’s committed-hash comparisons on the sidechain identify duplicate or outdated submissions, keeping perplexity low, with only a mild increase from 117.18 to 123.55.

These experiments further confirm that ZK-HybridFL’s sidechain-based validation and challenge mechanisms effectively prevent stale and malicious updates from influencing the global model. Additional experiments, including detailed ledger latency/throughput scaling, stake-weight ablations, and extended robustness studies, are provided in Sec. S3-C.

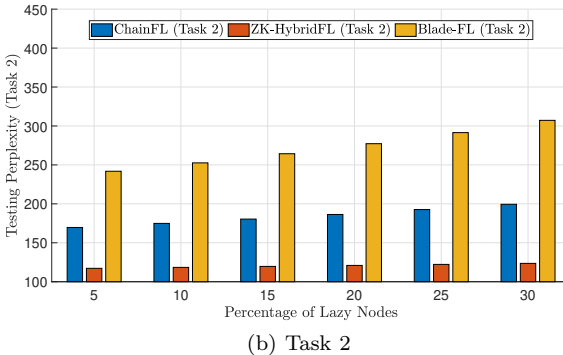
2) Ledger Perspective:

Latency and throughput: We measure latency as the average time to complete one global update round, from the start of local training until the corresponding block is integrated into the ledger. Throughput is the number of successful global update rounds completed by the network per minute; lower latency directly translates into higher throughput.

In ZK-HybridFL, latency is dominated by (i) local training and proof generation in Sec. IV-A1, (ii) parent selection and DAG updates in Sec. IV-A2, and (iii) occasional challenge resolution in Sec. IV-A3. SNARK verification and sidechain contract execution are lightweight (Sec. V-C3), so proof checking adds only milliseconds per tip model. The predict-then-prove workflow overlaps most



(a) Task 1



(b) Task 2

Fig. 8. Model performance versus lazy-node ratio γ for ZK-HybridFL, ChainFL, and Blade-FL with $n = 15$ and $\mu = 15\%$.

proof generation with subsequent training, further hiding ZKP costs. In ChainFL, latency is mainly driven by Raft-style consensus within each shard, whereas in Blade-FL it is dominated by the time spent solving proof-of-work (PoW) puzzles for block mining.

Figs. 9 and 10 summarize latency and throughput as the network scales from 5 to 30 nodes under $\mu = 20\%$ adversaries and $\gamma = 10\%$ lazy nodes. For Task 1, ZK-HybridFL maintains the lowest latency across all sizes (roughly 7.7–8.9 s), compared with 8.2–9.9 s for ChainFL and 9.1–10.2 s for Blade-FL. Task 2, which uses a heavier GRU model, exhibits higher latencies overall, but ZK-HybridFL again remains fastest (about 45.5–46.3 s) versus 51.4–52.3 s for ChainFL and 51.5–52.8 s for Blade-FL.

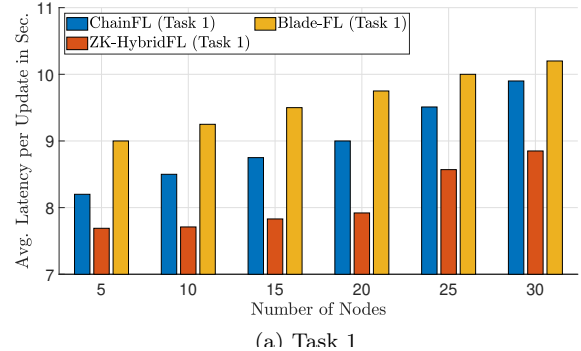
These latency gains translate into higher throughput. As Fig. 10 shows, ZK-HybridFL sustains the largest number of completed update rounds per minute for both tasks. The sidechain-based event-driven contracts and low-cost ZKP verification allow the DAG to remain uncongested, whereas ChainFL suffers from cross-shard synchronization and Blade-FL from PoW overhead as the network grows.

Scalability: We quantify scalability as the number of global epochs required for convergence. A global epoch is one full cycle in which all nodes perform local training and propagate their updates through the network. Let \mathcal{L}^t denote the training loss at epoch t . Convergence is declared when

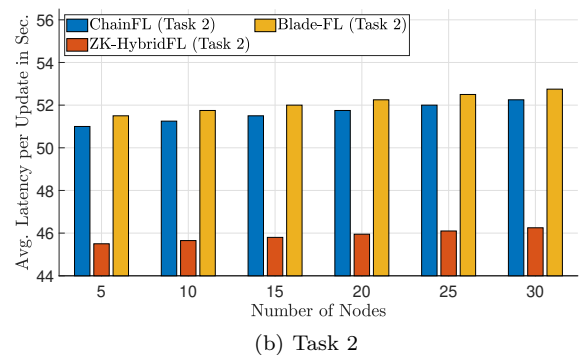
$$\frac{|\mathcal{L}^t - \mathcal{L}^{t-1}|}{\mathcal{L}^{t-1}} < \epsilon$$

holds for five consecutive epochs, with $\epsilon = 10^{-3}$.

Fig. 11 reports the number of epochs required to meet Sec. V-C2 as a function of n under $\mu = 20\%$

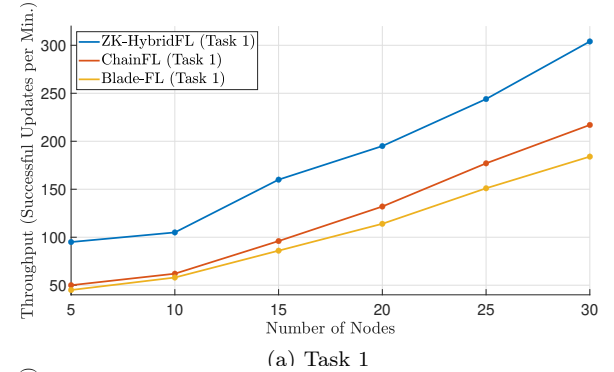


(a) Task 1

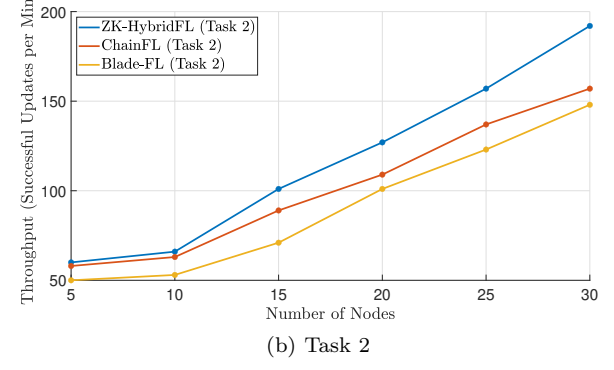


(b) Task 2

Fig. 9. Latency of Blade-FL, ChainFL, and ZK-HybridFL versus the number of nodes n with $\mu = 20\%$ adversarial nodes and $\gamma = 10\%$ lazy nodes.



(a) Task 1



(b) Task 2

Fig. 10. Throughput of Blade-FL, ChainFL, and ZK-HybridFL versus the number of nodes n with $\mu = 20\%$ adversarial nodes and $\gamma = 10\%$ lazy nodes.

adversarial and $\gamma = 10\%$ lazy nodes. For both tasks, ZK-HybridFL converges in the fewest epochs, ChainFL is intermediate, and Blade-FL requires the most. As n increases, adversarial and lazy behavior compounds the

TABLE II
Proof-generation cost per node (batch size $B = 10$).

Model	Params ($\times 10^3$)	FLOPs/sample ($\times 10^3$)	CPU prove (s)	GPU prove (s)	PK size (GB)
MLP-3k	3.6	3.5	3.2	0.51	0.16
CNN-20k	19.8	68	32	4.1	4.2
MobileNetV2-0.5	1300	3×10^5	665	76	31
GRU-256	29	950	360	44	4.3

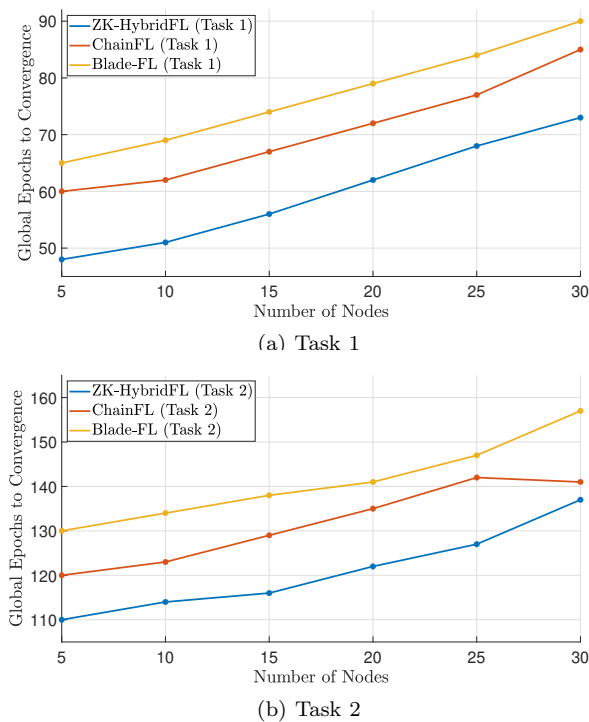


Fig. 11. Number of global epochs to convergence for Blade-FL, ChainFL, and ZK-HybridFL versus the number of nodes n with $\mu = 20\%$ adversarial nodes and $\gamma = 10\%$ lazy nodes.

weaknesses of Blade-FL’s PoW mechanism and ChainFL’s tip-based selection, forcing additional “recovery” epochs after corrupted updates. ZK-HybridFL, by pruning tainted or stale blocks via its challenge mechanism and loss-aware parent selection, avoids repeatedly training on compromised global models and thus reaches the convergence threshold significantly sooner.

3) Zero-Knowledge Proof Cost and Scalability: A key concern for ZK-HybridFL is the overhead of generating succinct noninteractive arguments of knowledge (SNARKs) for each node’s private validation batch. While on-chain verification is cheap, proof generation can be substantial for modern neural networks. We therefore benchmarked both proof and verification costs on the exact models used in our experiments, using a 16-core Intel Xeon Gold 6338 (3.0 GHz, 64 GB RAM) for central processing unit (CPU) runs and an NVIDIA A100 80 GB graphics processing unit (GPU) for accelerated proofs. Each node constructs a proof over a local test mini-batch of size $B = 10$, balancing statistical rigor and latency.

Table II summarizes proof-generation time, GPU speedup, and proving-key memory footprint for each model.

TABLE III
Proof-verification overhead.

Model	Verify time (s)	Proof size (KB)	Gas (k units)
MLP-3k	0.021	21	19
CNN-20k	0.028	17	21
MobileNetV2-0.5	0.095	118	24
GRU-256	0.108	41	23

Proof-generation time and memory footprint scale approximately linearly with the per-inference FLOPs. A small multilayer perceptron (MLP) with $\approx 3.6 \times 10^3$ parameters and 3.5×10^3 FLOPs per sample completes in 3.2s on CPU and 0.51s on GPU, with a 0.16 GB proving key. A GRU-256 (about 2.9×10^4 parameters and 9.5×10^5 FLOPs) requires 360s on CPU or 44s on GPU, with a 4.3 GB key. The largest model, MobileNetV2-0.5 ($\approx 1.3 \times 10^6$ parameters and 3×10^8 FLOPs), takes 665s on CPU or 76s on GPU, with a 31 GB key. For the GRU-256, GPU proof time scales roughly linearly with batch size, following $t_{\text{prove}} \approx 4.4B \pm 0.35s$ for $B \leq 40$.

SNARK verification, by contrast, is lightweight. Table III reports CPU verification time, proof size, and gas consumption on our Substrate test network. Verification completes in under 0.11s for all models, with proof sizes between 17 and 118 kB and gas costs between 19 k gas and 24 k gas. For a typical block-gas limit of 2×10^6 , publishing proofs from 30 participants consumes less than 1% of block capacity; storage fees are on the order of 5×10^{-5} token per proof.

The two additional proofs introduced in Sec. S1-B2 add only modest overhead on top of the base Groth16 proof. Table IV reports generation time, proof size, and gas for the Bulletproof Σ_j^t enforcing $L_t \leq \|\Delta \mathbf{W}_j^t\|_2 \leq B_t$ and the embedding-cosine SNARK Γ_j^t . Bulletproof proving time grows linearly with the number of parameters n ; even for MobileNetV2-0.5, the ℓ_2 -norm bound completes in about 26s on CPU or 2.6s on GPU. The cosine-check circuit is model-agnostic and yields a 0.2 kB proof in approximately 2.4s (CPU) or 0.30s (GPU). Verification costs are fixed at 38k gas for Σ_j^t and 25k gas for Γ_j^t , raising the total per-update gas from roughly 61k gas to 124k gas, still below 5% of a 2×10^6 -gas block for 30 concurrent trainers.

Thus, the extended proof bundle remains well within practical limits. Proof generation is overlapped with training via the predict-then-prove workflow (cf. Sec. II-A), and on-chain verification occupies less than 5% of block gas while adding negligible latency relative to consensus. Models that require more than 24 GB of GPU memory for proving keys can use tensorplonk paging (512 MiB chunks) to stream keys from CPU RAM with under

TABLE IV
Incremental proofs: generation and verification cost (same hardware as Tables II and III).

Proof	CPU prove	GPU prove	Proof size	Verify gas	Dependence on n
ℓ_2 -BP, MLP-3k	0.07 s	0.008 s	1.6 kB	38 k	linear
ℓ_2 -BP, CNN-20k	0.4 s	0.05 s	2.3 kB	38 k	linear
ℓ_2 -BP, GRU-256	0.6 s	0.08 s	2.8 kB	38 k	linear
ℓ_2 -BP, MobileNetV2-0.5	26 s	2.6 s	8.1 kB	38 k	linear
Cosine-SNARK (all models)	2.4 s	0.30 s	0.2 kB	25 k	constant

5% overhead, or employ recursive folding (e.g., Halo Infinite) to partition large circuits into subproofs with sub-20 GB keys, recombined on chain with only ≈ 20 ms additional verification time. A detailed implementation and performance analysis of a GRU-256 model using recursive folding is provided in the supplementary material (Sec. S3-B).

VI. Conclusions

We presented ZK-HybridFL, a secure decentralized federated learning framework integrating a DAG ledger, sidechain smart contracts, and zero-knowledge proofs for privacy-preserving, robust validation. Across image and text tasks, it outperforms Blade-FL and ChainFL, while delivering lower latency and higher throughput than proof-of-work or leader-based systems. Its challenge mechanism prunes invalid updates to accelerate convergence and reduce epochs. Future work will refine the cryptographic design and evaluate edge deployments.

References

- [1] S. Hong and J. Chae, “Distributed online learning with multiple kernels,” *IEEE Trans. Neural Netw. Learn. Syst.*, vol. 34, no. 3, pp. 1263–1277, Mar. 2023, doi:10.1109/TNNLS.2021.3105146.
- [2] A. P. Kalapaaking, I. Khalil, X. Yi, K.-Y. Lam, G.-B. Huang, and N. Wang, “Auditable and verifiable federated learning based on blockchain-enabled decentralization,” *IEEE Trans. Neural Netw. Learn. Syst.*, vol. 36, no. 1, pp. 102–115, Jan. 2025, doi:10.1109/TNNLS.2024.3407670.
- [3] G. Yu et al., “IronForge: An open, secure, fair, decentralized federated learning,” *IEEE Trans. Neural Netw. Learn. Syst.*, vol. 36, no. 1, pp. 354–368, Jan. 2025, doi:10.1109/TNNLS.2023.3329249.
- [4] H. Kim, J. Park, M. Bennis, and S.-L. Kim, “Blockchain-based on-device federated learning,” *IEEE Commun. Lett.*, vol. 24, no. 6, pp. 1279–1283, Jun. 2020, doi:10.1109/LCOMM.2019.2921755.
- [5] S. Zhou, H. Huang, W. Chen, P. Zhou, Z. Zheng, and S. Guo, “PIRATE: A blockchain-based secure framework of distributed machine learning in 5G networks,” *IEEE Netw.*, vol. 34, no. 6, pp. 84–91, Nov./Dec. 2020, doi:10.1109/MNET.001.1900658.
- [6] E. Baccarelli, M. Scarpiniti, A. Momenzadeh, and S. S. Ahrabi, “AFAFed—Asynchronous fair adaptive federated learning for IoT stream applications,” *Comput. Commun.*, vol. 195, pp. 376–402, Nov. 2022.
- [7] K. E. Tan, “Achieving security and privacy in federated learning systems: Survey, research challenges and future directions,” *Eng. Appl. Artif. Intell.*, vol. 106, Art. no. 104468, Nov. 2021.
- [8] X. Cheng, W. Tian, F. Shi, M. Zhao, S. Chen, and H. Wang, “A blockchain-empowered cluster-based federated learning model for blade icing estimation on IoT-enabled wind turbine,” *IEEE Trans. Ind. Informat.*, vol. 18, no. 12, pp. 9184–9195, Dec. 2022.
- [9] L. Cui, X. Su, and Y. Zhou, “A fast blockchain-based federated learning framework with compressed communications,” *IEEE J. Sel. Areas Commun.*, vol. 40, no. 12, pp. 3358–3372, Dec. 2022.
- [10] C. Feng, B. Liu, K. Yu, S. K. Goudos, and S. Wan, “Blockchain empowered decentralized horizontal federated learning for 5G-enabled UAVs,” *IEEE Trans. Ind. Informat.*, vol. 18, no. 5, pp. 3582–3592, May 2021.
- [11] A. Imteaj, M. H. Amini, and P. M. Pardalos, *Foundations of Blockchain: Theory and Applications*. Cham, Switzerland: Springer, 2021.
- [12] D. C. Nguyen et al., “Federated learning meets blockchain in edge computing: Opportunities and challenges,” *IEEE Internet Things J.*, vol. 8, no. 16, pp. 12806–12825, Aug. 2021.
- [13] S. Wang et al., “Adaptive federated learning in resource constrained edge computing systems,” *IEEE J. Sel. Areas Commun.*, vol. 37, no. 6, pp. 1205–1221, Jun. 2019.
- [14] A. Taherpour and X. Wang, “A high-throughput and secure coded blockchain for IoT,” *IEEE Transactions on Dependable and Secure Computing*, vol. 22, no. 4, pp. 3561–3579, Jul.–Aug. 2025, doi: 10.1109/TDSC.2025.3532850.
- [15] Z. Luan, W. Li, M. Liu, and B. Chen, “Robust federated learning: Maximum correntropy aggregation against Byzantine attacks,” *IEEE Trans. Neural Netw. Learn. Syst.*, vol. 36, no. 1, pp. 62–75, Jan. 2025, doi:10.1109/TNNLS.2024.3383294.
- [16] X. Tang, M. Shen, Q. Li, L. Zhu, T. Xue, and Q. Qu, “PILE: Robust privacy-preserving federated learning via verifiable perturbations,” *IEEE Trans. Dependable Secure Comput.*, vol. 20, no. 6, pp. 5005–5023, Nov./Dec. 2023, doi:10.1109/TDSC.2023.3239007.
- [17] A. Taherpour and X. Wang, “HybridChain: Fast, accurate, and secure transaction processing with distributed learning,” *IEEE Transactions on Parallel and Distributed Systems*, vol. 35, no. 6, pp. 968–982, Jun. 2024, doi: 10.1109/TPDS.2024.3381593.
- [18] A. Taherpour and X. Wang, “SPID-Chain: A smart contract-enabled, polar-coded interoperable DAG chain,” *arXiv preprint arXiv:2501.11794 [cs.DC]*, Jan. 2025, doi: 10.48550/arXiv.2501.11794.
- [19] L. Zhu, Z. Liu, and S. Han, “Deep leakage from gradients,” in *Advances in Neural Information Processing Systems (NeurIPS)*, vol. 32, 2019.
- [20] X. Luo, Y. Wu, X. Xiao, and B. C. Ooi, “Feature inference attack on model predictions in vertical federated learning,” in *Proc. 2021 IEEE 37th Int. Conf. Data Eng. (ICDE)*, 2021, pp. 181–192.
- [21] M. Lam, G.-Y. Wei, D. Brooks, V. J. Reddi, and M. Mitzenmacher, “Gradient disaggregation: Breaking privacy in federated learning by reconstructing the user participant matrix,” in *Proc. Int. Conf. Mach. Learn. (ICML)*, PMLR, 2021, pp. 5959–5968.
- [22] M. Abadi, A. Chu, I. Goodfellow, H. B. McMahan, I. Mironov, K. Talwar, and L. Zhang, “Deep learning with differential privacy,” in *Proc. 2016 ACM SIGSAC Conf. Comput. Commun. Security (CCS)*, 2016, pp. 308–318.
- [23] K. Tam, L. Li, B. Han, C. Xu, and H. Fu, “Federated noisy client learning,” *IEEE Trans. Neural Netw. Learn. Syst.*, vol. 36, no. 1, pp. 1799–1812, Jan. 2025, doi:10.1109/TNNLS.2023.3336050.
- [24] J. Li et al., “Blockchain assisted decentralized federated learning (BLADE-FL): Performance analysis and resource allocation,” *IEEE Trans. Parallel Distrib. Syst.*, vol. 33, no. 10, pp. 2401–2415, Oct. 2022, doi:10.1109/TPDS.2021.3138848.
- [25] S. Yuan, B. Cao, Y. Sun, Z. Wan, and M. Peng, “Secure and efficient federated learning through layering and sharding blockchain,” *IEEE Trans. Netw. Sci. Eng.*, vol. 11, no. 3, pp. 3120–3134, May/Jun. 2024, doi:10.1109/TNSE.2024.3361458.
- [26] H. Wang, Y. Yu, and Y. Jiang, “Fully decentralized multiagent communication via causal inference,” *IEEE Trans. Neural Netw. Learn. Syst.*, vol. 34, no. 12, pp. 10193–10202, Dec. 2023, doi:10.1109/TNNLS.2022.3165114.
- [27] T. Liu, X. Xie, and Y. Zhang, “ZkCNN: Zero knowledge proofs for convolutional neural network predictions and accuracy,” in

- Proc. 2021 ACM SIGSAC Conf. Comput. Commun. Security (CCS), 2021, pp. 2968–2985.
- [28] T. Ruckel, J. Sedlmeir, and P. Hofmann, “Fairness, integrity, and privacy in a scalable blockchain-based federated learning system,” *Comput. Netw.*, vol. 202, Art. no. 108621, 2022.
- [29] B. Feng, L. Qin, Z. Zhang, Y. Ding, and S. Chu, “Zen: An optimizing compiler for verifiable, zero-knowledge neural network inferences,” *arXiv*, 2021. [Online]. Available: <https://arxiv.org/abs/2105.09130>
- [30] F. McKeen et al., “Innovative instructions and software model for isolated execution,” in Proc. 2nd Int. Workshop on Hardware and Architectural Support for Security and Privacy (HASP), 2013, pp. 10–16, doi:10.1145/2487726.2488368.
- [31] R. Poddar, T. Bozic, R. A. Popa, and I. Stoica, “Verifiable oblivious storage,” in Proc. 2019 ACM SIGSAC Conf. Comput. Commun. Security (CCS), 2019, pp. 1699–1716, doi:10.1145/3319535.3354214.
- [32] J. Groth, “On the size of pairing-based non-interactive arguments,” in *Advances in Cryptology—EUROCRYPT 2016*, vol. 9665. Springer, 2016, pp. 305–326.
- [33] B. Parno, C. Gentry, J. Howell, and M. Raykova, “Pinocchio: Nearly practical verifiable computation,” in Proc. 2013 IEEE Symp. Security and Privacy (SP), 2013, pp. 238–252, doi:10.1109/SP.2013.47.
- [34] A. De Santis and G. Persiano, “Zero-knowledge proofs of knowledge without interaction,” in Proc. 33rd Annu. Symp. Foundations of Computer Science (FOCS), 1992, pp. 427–436, doi:10.1109/SFCS.1992.267809.
- [35] P. Ghosh, “The state-of-the-art in zero-knowledge authentication proof for cloud,” in *Machine Learning Techniques and Analytics for Cloud Security*. Wiley, 2022, pp. 149–170, doi:10.1002/9781119764113.ch8.
- [36] S. Müller, A. Penzkofer, N. Polyanskii, J. Theis, W. Sanders, and H. Moog, “Tangle 2.0: Leaderless Nakamoto consensus on the heaviest DAG,” *IEEE Access*, vol. 10, pp. 105807–105842, 2022, doi:10.1109/ACCESS.2022.3196538.
- [37] D. Dziubaltowska, “The security of the Coordicide: The implementation and analysis of possible attack vectors,” *arXiv*, 2022. [Online]. Available: <https://arxiv.org/abs/2205.12568>
- [38] M. Döring, “Simple, strict, proper, and directed: Comparing reachability in directed and undirected temporal graphs,” *arXiv*, Jan. 2025. [Online]. Available: <https://arxiv.org/abs/2501.11697>
- [39] G. Kritikakis and I. G. Tollis, “Fast and practical DAG decomposition with reachability applications,” *arXiv*, Dec. 2022. [Online]. Available: <https://arxiv.org/abs/2212.03945>
- [40] N. Boria, G. Cabodi, P. Camurati, M. Palena, P. Pasini, and S. Quer, “A greedy approach to answer reachability queries on DAGs,” *arXiv*, Nov. 2016. [Online]. Available: <https://arxiv.org/abs/1611.02506>
- [41] H. Song, Y. Wei, Z. Qu, and W. Wang, “Unveiling decentralization: A comprehensive review of technologies, comparison, challenges in Bitcoin, Ethereum, and Solana blockchain,” *arXiv*, Apr. 2024. [Online]. Available: <https://arxiv.org/abs/2404.04841>
- [42] L. Lamport, “Time, clocks, and the ordering of events in a distributed system,” *Commun. ACM*, vol. 21, no. 7, pp. 558–565, Jul. 1978.
- [43] R. K. Ghosh and H. Ghosh, “Clock synchronization and event ordering,” in *Distributed Systems: Theory and Applications*. Wiley-IEEE Press, 2023, pp. 91–125, doi:10.1002/9781119825968.ch5.
- [44] E. Shao, “BLADE-FL: Blockchain assisted decentralized federated learning,” GitHub repository, 2020. [Online]. Available: <https://github.com/ElvisShaoYumeng/BLADE-FL>
- [45] S. Yuan, “ChainsFL: A blockchain-based federated learning implementation,” GitHub repository, 2021. [Online]. Available: <https://github.com/shuoyuan/ChainsFL-implementation>
- [46] TensorFlow, “TensorFlow Federated: Machine learning on decentralized data.” [Online]. Available: <https://www.tensorflow.org/federated>
- [47] IOTA Foundation, “GoShimmer Docker Network Tool,” GitHub repository, 2023. [Online]. Available: <https://github.com/iotaledger/goshimmer/tree/develop/tools/docker-network>
- [48] Parity Technologies, “Substrate: The blockchain framework for a multichain future.” [Online]. Available: <https://substrate.io/>
- [49] World Wide Web Consortium (W3C), “WebAssembly.” [Online]. Available: <https://webassembly.org/>
- [50] gRPC Authors, “gRPC: A high-performance, open-source universal RPC framework.” [Online]. Available: <https://grpc.io/>
- [51] Apache Software Foundation, “Apache Kafka: A distributed streaming platform.” [Online]. Available: <https://kafka.apache.org/>
- [52] ZKondut, “ezkl: Easy zero-knowledge inference,” GitHub repository, 2023. [Online]. Available: <https://github.com/zkondut/ezkl>
- [53] D. Kang, T. Hashimoto, I. Stoica, and Y. Sun, “zkml: Trustless machine learning for all,” GitHub repository, 2023. [Online]. Available: <https://github.com/ddkang/zkml>
- [54] M. Sandler, A. Howard, M. Zhu, A. Zhmoginov, and L.-C. Chen, “MobileNetV2: Inverted residuals and linear bottlenecks,” in Proc. IEEE Conf. Comput. Vis. Pattern Recognit. (CVPR), 2018, pp. 4510–4520, doi:10.1109/CVPR.2018.00474.

Supplementary

S1. Cryptographic Protocols and Security Analysis

This section details the cryptographic foundations of the ZK-HybridFL system. It begins by specifying the concrete implementations of the zero-knowledge proofs, including KZG commitments and Groth16 SNARKs. It then introduces an expanded threat model with more subtle attacks and presents an extended ZKP bundle, which incorporates additional proofs such as Bulletproofs, as a countermeasure. The section concludes with a formal security analysis of these extended defenses against collusion and various privacy attacks.

A. Zero-Knowledge Proofs: Instantiation and Extensions

1) Cryptographic Instantiation: The generic workflow above abstracts away the precise commitment scheme and the algebraic details of the SNARK. We now spell out the concrete instantiation used in our implementation.

Polynomial commitments: Let $\mathbf{W}_j^t \in \mathbb{F}_p^n$ be the trainer's weight tensor at round t , flattened into the length- n vector

$$\mathbf{W}_j^t = (W_{j,0}^t, W_{j,1}^t, \dots, W_{j,n-1}^t),$$

where each $W_{j,i}^t \in \mathbb{F}_p$ is one scalar model parameter. Similarly, let the test-batch tensor $D_j^{t,\text{test}} \in \mathbb{F}_p^m$ be flattened as

$$D_j^{t,\text{test}} = (D_{j,0}^{t,\text{test}}, D_{j,1}^{t,\text{test}}, \dots, D_{j,m-1}^{t,\text{test}}),$$

with each $D_{j,i}^{t,\text{test}} \in \mathbb{F}_p$ denoting one scalar feature or label value in the batch.

We then interpret these as evaluation vectors of degree- $(n-1)$ and degree- $(m-1)$ polynomials in $\mathbb{F}_p[x]$:

$$\begin{aligned} f_W(x) &= \sum_{i=0}^{n-1} W_{j,i}^t x^i, \\ f_D(x) &= \sum_{i=0}^{m-1} D_{j,i}^{t,\text{test}} x^i, \\ f_W, f_D &\in \mathbb{F}_p[x]. \end{aligned}$$

Under the KZG setup (secret $\tau \in \mathbb{F}_p$), we commit by

$$C_j^{t,\text{model}} = g_1^{f_W(\tau)}, \quad C_j^{t,\text{test}} = g_1^{f_D(\tau)}.$$

Each commitment is a single 48-byte point in \mathbb{G}_1 and is stored on the sidechain together with a Lamport timestamp (see Sec. S2-A2).

Trusted setup: A single powers-of-tau ceremony produces (i) the universal structured reference string $(g_1^{\tau^k})_{k=0}^{k_{\max}}$ and (ii) the circuit-specific proving key \mathbf{pk} and verification key \mathbf{vk} for the Groth16 SNARK. The ceremony is executed once at task deployment; afterwards \mathbf{pk} is distributed off-chain to trainers, whereas \mathbf{vk} is pinned on-chain.

Non-interactive proof: As described in the main-text ZK workflow (Sec. II-A), using \mathbf{pk} , trainer j computes a Groth16 proof Π_j^t based on public inputs. Since the Fiat-Shamir heuristic is applied to derive challenges deterministically, no additional interaction or exchange of randomness is required.

Verification contract: The sidechain validator performs:

- (i) Two KZG opening checks (two pairings and one multi-exponentiation; cost ≈ 34.2 k gas and 144 B of storage for the two 48-byte commitments),
- (ii) One Groth16 verification call on $(C_j^{t,\text{model}}, C_j^{t,\text{test}}, \mathcal{Y}_j^t, \mathcal{L}_j^t, \Pi_j^t)$ (cost 20–27 k gas; see Table III).

Even with 30 trainers, this, plus the additional 144 B of on-chain storage, remains under 1% of a 2 M gas block, keeping overhead negligible. If all checks succeed, a `ProofOK` event is emitted. Otherwise, the update is rejected and node j 's stake becomes challengeable.

Asynchronous epochs: Immediately after publishing their commitments $(C_j^{t,\text{model}}, C_j^{t,\text{test}})$, each trainer resumes the next SGD epoch while proof generation runs concurrently (the “predict-then-prove” schedule). We allow a two-epoch grace window, which is sufficient even for a 76 s GPU proof for MobileNetV2-0.5 on MNIST (each epoch itself takes 24 s to 30 s). Commitments and proofs carry Lamport timestamps to totally order sidechain events, so late proofs simply land in the next round without any global pause (see Sec. S2-A2).

2) Security Guarantees: The combination of KZG commitments and Groth16 delivers the usual completeness, soundness, and zero-knowledge properties. Below we make those guarantees explicit for the concrete operations performed in ZK-HybridFL.

Model or data substitution: Let $C_j^{t,\text{model}}$ and $C_j^{t,\text{test}}$ be the commitments posted in step (i) of Sec. S1-A1, and let $\Pi = \Pi_j^t$ be the proof broadcast in step (iii). Suppose the prover attempts to convince the verifier with an altered model $\tilde{\mathbf{W}} \neq \mathbf{W}_j^t$ or test batch $\tilde{D} \neq D_j^{t,\text{test}}$. Because KZG is binding, the pair of polynomials $(f_{\tilde{W}}, f_{\tilde{D}})$ cannot both satisfy

$$g_1^{f_{\tilde{W}}(\tau)} = C_j^{t,\text{model}} \quad \text{and} \quad g_1^{f_{\tilde{D}}(\tau)} = C_j^{t,\text{test}},$$

so at least one KZG-opening check fails and verification returns 0.

Fabricating outputs or loss: Suppose instead the prover keeps the committed witness $(\mathbf{W}_j^t, D_j^{t,\text{test}})$ but replaces the public outputs by $\tilde{\mathcal{Y}} \neq \mathcal{Y}_j^t$ or $\tilde{\mathcal{L}} \neq \mathcal{L}_j^t$. The algebraic relations embedded in the Groth16 circuit bind the full witness \mathcal{U}_j^t to the declared outputs, so any mismatch violates a circuit constraint and forces the SNARK verifier to return 0.

Lazy-node detection: Each bundle Z_j^t includes the hash $\mathsf{H}(\mathcal{Y}_j^t)$ alongside $C_j^{t,\text{model}}$ and $C_j^{t,\text{test}}$. Because both KZG and H are collision-resistant, two bundles that replay an identical prediction vector must derive from the same (\mathbf{W}, D) witness (and thus the same loss). Smart contract S_j^1 cross-checks these hashes across the DAG: any node that replays an old model to avoid fresh training is flagged and its update excluded from the parent-selection ranking (cf. Sec. III-A1), mitigating lazy-node attacks.

Consistency across forks: KZG commitments and the hash $\mathsf{H}(\mathcal{Y})$ are stored in the immutable part of the sidechain; therefore every honest replica of the DAG sees exactly

the same triplet $(C^{t,\text{model}}, C^{t,\text{test}}, \mathsf{H}(\mathcal{Y}))$. This global consistency enables (i) deterministic parent selection and (ii) unambiguous fork resolution, even under short-lived network forks.

Taken together, these properties ensure that only genuinely trained, fully verified updates influence the global model, while any adversarial attempt, whether by parameter substitution, fabricated outputs, or stale replay is detected and rejected except with negligible probability.

B. Extended ZKP Defenses

1) Broader Threat Model: While the core workflow of Sec. II-A ensures that blatantly bogus updates (e.g., completely untrained models, fabricated outputs, or exact replays) are caught with overwhelming probability, a realistic threat model must also consider subtler strategies that deliberately skirt these checks. Below, we sketch three attack avenues that slip through the ZKP workflow in Sec. II-A.

First, a node skips training altogether and re-posts an older weight tensor $\mathbf{W}_j^{t-\Delta}$ with a microscopic perturbation. This changes the hash of the predictions, so replay detection in Sec. II-A does not trigger, but the global model sees no genuine progress.

Second, instead of performing full local SGD, the node applies a single gradient step $\delta\mathbf{W}$ and then scales it by a tiny factor α . The resulting update $\mathbf{W}_j^{t-1} + \alpha\delta\mathbf{W}$ meets the norm bound and earns the block reward, yet makes negligible impact on the model’s decision surface.

Third, since the test batch $D_j^{t,\text{test}}$ is chosen privately, a malicious trainer can cherry-pick samples on which \mathbf{W}_j^t already performs well, or even craft an easy synthetic set, then prove the accuracy honestly. The ZKP verifies, but the reported loss overstates the model’s real-world quality.

To address these security gaps, next we introduce lightweight extensions that detect and penalize the three strategies above, without reshaping the Groth16-based core.

2) Extended ZKP Bundle: In each training epoch t , we extend the original Z-bundle from Sec. II-A with two lightweight, non-interactive proofs to ensure that every submitted update both moves the weights by a meaningful amount and alters the model’s internal representations. The efficiency of these methods has been demonstrated in [7], [8]. We defer a detailed security analysis of these extended ZKPs to Sec. S1-C.

Specifically, in epoch t , each client j is given the public thresholds $[L_t, B_t]$ and τ_{\max} . See Sec. S2-B1 for how these thresholds are computed and how consensus is reached across the network through interactions with the oracle committee, sidechain, and smart contracts.

With these parameters in hand, each node j proceeds as follows in epoch t :

1) Constructs the original Z-bundle.

The node first performs standard local training and generates a Groth16 proof Π_j^t verifying inference cor-

rectness. It then commits the model and test data and assembles the initial Z-bundle:

$$Z_j^t = \left(\Pi_j^t, \mathcal{Y}_j^t, \mathcal{L}_j^t, C_j^{t,\text{model}}, C_j^{t,\text{test}} \right).$$

2) Proves the norm of the update with Bulletproofs.

To ensure that the weight change is non-trivial, the node computes the update $\Delta\mathbf{W}_j^t = \mathbf{W}_j^t - \mathbf{W}_j^{t-1}$ and produces a range proof (Bulletproof)

$$\Sigma_j^t = \text{BPProve}(\Delta\mathbf{W}_j^t, L_t, B_t).$$

This proof references the existing commitment $C_j^{t,\text{model}}$ to link the norm constraint to the committed model.

3) Attests to semantic change using embedding-cosine SNARK.

The node computes layer- ℓ activations over a public probe set:

$$\mathbf{z}_{\text{old}} = \frac{1}{|D_{\text{probe}}|} \sum_{x \in D_{\text{probe}}} \phi_{\ell}(\mathbf{W}_j^{t-1}, x),$$

$$\mathbf{z}_{\text{new}} = \frac{1}{|D_{\text{probe}}|} \sum_{x \in D_{\text{probe}}} \phi_{\ell}(\mathbf{W}_j^t, x),$$

and generates a SNARK proving $\cos(\mathbf{z}_{\text{old}}, \mathbf{z}_{\text{new}}) \leq \tau_{\max}$:

$$\Gamma_j^t = \text{SNARKProve}(\cos(\mathbf{z}_{\text{old}}, \mathbf{z}_{\text{new}}) \leq \tau_{\max}; C_{\text{probe}}).$$

4) Assembles the extended bundle.

The node merges the original bundle with the two additional proofs:

$$Z_j^{t,\text{ext}} = Z_j^t \parallel \Sigma_j^t \parallel \Gamma_j^t$$

$$= \left(\Pi_j^t, \Sigma_j^t, \Gamma_j^t, \mathcal{Y}_j^t, \mathcal{L}_j^t, C_j^{t,\text{model}}, C_j^{t,\text{test}} \right).$$

5) Submits for peer or on-chain verification.

A verifier node j' or the chain checks all parts in order:

- a) $\text{VerifyGroth16}(\mathbf{vk}, \Pi_j^t, C_j^{t,\text{model}}, C_j^{t,\text{test}}, \mathcal{Y}_j^t, \mathcal{L}_j^t),$
- b) $\text{VerifyBulletproof}(\Sigma_j^t; C_j^{t,\text{model}}),$
- c) $\text{VerifyCosineZKP}(\Gamma_j^t; C_{\text{probe}}).$

The update is accepted into the DAG only if all verifications succeed.

Note that Σ_j^t must reference $C_j^{t,\text{model}}$ so that the norm bound applies to the committed weights, and Γ_j^t refers to the fixed public probe-set commitment C_{probe} . No additional commitments are required.

Moreover, in addition to the two KZG openings (approximately 34.2 k gas) and the Groth16 verification (20–27 k gas), each update in the extended scheme carries:

- A Bulletproof Σ_j^t for the ℓ_2 -bound (proof size ≈ 8.1 kB off-chain), which costs ≈ 38 k gas to verify.
- An embedding-cosine SNARK Γ_j^t (proof size ≈ 200 B), which costs ≈ 25 k gas to verify.

Taken together, the two new verifications add roughly 63 k gas, under 3.2% of a 2 M gas block, on top of the original ≈ 61 k gas, keeping total overhead below 5% of block capacity; see Table IV for a full breakdown.

Remark S1.1. Although we have extended the original Z-bundle, the underlying DAG ledger and its consensus rules

(Sec. II-B) remain unchanged. Likewise, the challenge mechanism of Sec. II-C applies verbatim to each extended bundle: any node may still issue and resolve challenges against $Z_j^{t,\text{ext}}$ under the same stake-based rules.

C. Extended Security Analysis

Let $\text{Accept}_t(D_j(t)) \in \{0, 1\}$ be the sidechain predicate that a candidate block $D_j(t)$ is eventually confirmed and its model \mathbf{W}_j^t enters the global aggregation of epoch t (cf. Sec. II-A–Sec. III). An adversarial trainer replaces the honest map

$$\mathcal{T} : (\mathbf{W}_j^{t-1}, \mathcal{D}_j^{t,\text{train}}) \mapsto \mathbf{W}_j^t$$

by $\tilde{\mathcal{T}}$ and tries to maximise $\Pr[\text{Accept}_t(D_j(t)) = 1]$ while breaking at least one of

1. Freshness – the update should encode genuine computation;
2. Correctness – the loss/accuracy in Z_j^t must be truthful;
3. Privacy – the attack must not leak information that enables model inversion or membership inference.

Extended ZKP Attack Defenses: We formalise three subtle strategies and prove that, once the extended Z-bundle $(\Pi \parallel \Sigma \parallel \Gamma)$ is enabled, each is rejected with probability $\text{negl}(\lambda)$, where $\lambda = 128$ is the global security parameter.

Attack $\mathcal{A}_{\text{lazy}}$ (Perturb–Replay). The node skips training and publishes

$$\mathbf{W}_j^t = \mathbf{W}_j^{t-\Delta} + \boldsymbol{\eta}, \quad \boldsymbol{\eta} \sim \mathcal{N}(\mathbf{0}, \sigma^2 \mathbf{I}),$$

with $\Delta \geq 1$ and $\|\boldsymbol{\eta}\|_2 \ll \|\mathbf{W}_j^{t-\Delta}\|_2$, so the prediction hash changes but \mathbf{W}_j^t is semantically identical to an old model.

Defence. If $C_j^{t,\text{model}}$ equals the old commitment, the replay filter of Sec. II-A fires. Otherwise Σ_j^t proves $L_t \leq \|\mathbf{W}_j^t - \mathbf{W}_j^{t-1}\|_2 = \|\boldsymbol{\eta}\|_2 \leq B_t$. By choosing σ so that $\Pr[\|\boldsymbol{\eta}\|_2 \geq L_t] \leq 2^{-128}$, the attack succeeds only with negligible probability.

Attack $\mathcal{A}_{\text{scale}}$ (Minimal-Norm Stalling). Compute one honest gradient $\delta\mathbf{W}$ and publish

$$\mathbf{W}_j^t = \mathbf{W}_j^{t-1} + \alpha \delta\mathbf{W}$$

with $\alpha = L_t / \|\delta\mathbf{W}\|_2$, so Σ_j^t passes but the semantic change is tiny.

Defence. Let $\bar{\mathbf{z}}_\ell(\mathbf{W})$ be the average layer- ℓ activation on the fixed $|D_{\text{probe}}|=400$ public probe samples. From [8] this map is κ -Lipschitz: $\|\bar{\mathbf{z}}_\ell(\mathbf{W} + \Delta) - \bar{\mathbf{z}}_\ell(\mathbf{W})\|_2 \leq \kappa \|\Delta\|_2$. Hence

$$\cos(\bar{\mathbf{z}}_\ell(\mathbf{W}_j^{t-1}), \bar{\mathbf{z}}_\ell(\mathbf{W}_j^t)) \leq 1 - \frac{\kappa^2 L_t^2}{2 \|\bar{\mathbf{z}}_\ell(\mathbf{W}_j^{t-1})\|_2^2} < \tau_{\text{max}},$$

whenever $\kappa L_t > (1 - \tau_{\text{max}})$. The inequality holds for our empirical choice $\kappa \approx 0.14$, $\tau_{\text{max}} = 0.98$, $L_t \geq 10^{-2}$. Thus the embedding-cosine SNARK Γ_j^t fails and $\text{Accept}_t = 0$.

Attack $\mathcal{A}_{\text{priv}}$ (Private-Test Cherry Pick). Keep \mathbf{W}_j^t honest but choose $\tilde{\mathcal{D}}_j^{t,\text{test}}$ to inflate the reported accuracy.

Defence. (i) The block’s rank in the parent-selection list (Sec. III-A1) depends on \mathcal{L}_j^t . By inflating accuracy (lower loss) the adversary increases the probability that

its own block is selected; this is not obviously harmful yet exposes the block to scrutiny. (ii) Before aggregation, any node evaluates the public probe set; if the empirical loss differs by more than $\varepsilon_{\text{probe}} = 0.01$ from the stated \mathcal{L}_j^t , it files a challenge (Sec. II-C). The honest majority of oracles detects the mismatch with constant probability $p_{\text{det}} \geq 1/2$, so the expected stake loss per dishonest epoch is at least $p_{\text{det}} \cdot s_{\text{min}}$, where s_{min} is the minimum slashing fraction. After $T \geq (\omega_j^0 / s_{\text{min}}) / p_{\text{det}} = O(\lambda)$ epochs, the attacker’s weight drops below the confirmation threshold and its updates are ignored. Thus

$$\Pr[\text{Accept}_t = 1 \wedge |\hat{\mathcal{L}}_{\text{probe}} - \mathcal{L}_j^t| > \varepsilon_{\text{probe}}] \leq \text{negl}(\lambda).$$

Thus, combining binding of KZG commitments, knowledge-soundness of Groth16/Bulletproof/SNARK proofs, and the economic penalty from the challenge mechanism yields

$$\Pr[\exists t, j : \text{Accept}_t(D_j(t)) = 1 \wedge D_j(t) \text{ is adversarial}] = \text{negl}(\lambda). \quad \square$$

Additional Privacy and Collusion Threats: Collusion-induced weight inflation

Attack \mathcal{A}_{col} . A coalition $\mathcal{C} \subseteq \{1, \dots, n\}$ with total stake $\Omega_{\mathcal{C}} = \sum_{j \in \mathcal{C}} \omega_j$ tries to force an invalid block B_{adv} into the confirmed set by (i) cross-verifying each other’s proofs and (ii) recursively selecting B_{adv} as an ancestor so that its AW eventually exceeds the confirmation threshold η (Sec. II-B).

Lemma S1.2 (Bounded-stake collusion). Let M be the oracle-committee size and assume $M \geq 3f + 1$ with at most f Byzantine oracles ($> 2/3$ honest stake). If $\Omega_{\mathcal{C}} < \eta/3$ then

$$\Pr[B_{\text{adv}} \text{ confirmed}] = \text{negl}(\lambda).$$

Sketch. Every new block needs a threshold-signed EventApproved log. Because at least $f + 1$ honest oracles must co-sign, an invalid B_{adv} can be published only if at least one honest oracle is fooled by a forged SNARK; the soundness error of Groth16 is $\varepsilon_{\text{SNARK}} \leq 2^{-\lambda}$. Subsequent children add at most $\Omega_{\mathcal{C}}$ weight each, so after k rounds the total AW on B_{adv} is bounded by $\Omega_{\mathcal{C}} k < k \eta/3$. But at least k honest blocks appear in the same future cone, contributing $k(1 - \Omega_{\mathcal{C}}) > 2k\eta/3$, so B_{adv} can never reach η . A full proof follows standard PBFT stake-counting (Sec. V-C2). \square

Remark S1.3. ZK-HybridFL is collusion-resistant as long as the adversary controls less than $\eta/3$ stake and less than $\frac{1}{3}$ of the oracle committee, matching the usual BFT threshold.

Model-inversion attacks

Threat. Given the public trajectory $\{\tilde{\mathbf{W}}^t\}_{t \leq T}$, an adversary solves an optimisation

$$\hat{\mathbf{x}} = \arg \min_{\mathbf{z}} \sum_t \|\nabla_{\mathbf{W}} \mathcal{L}(\tilde{\mathbf{W}}^t; \mathbf{z}) - \nabla_{\mathbf{W}} \mathcal{L}(\tilde{\mathbf{W}}^t; \mathbf{x})\|_2^2$$

to reconstruct a private training point \mathbf{x} [12], [13].

Baseline mitigation. ZK-HybridFL never discloses gradients; only final weights are visible. Empirically, inversion

from weights is far noisier than from per-step gradients [14]. Nevertheless the risk is not cryptographically closed.

Plug-in defences (future work). The pipeline is orthogonal to: (i) DP-SGD noise addition [14], [15]; (ii) secure aggregation of weights [16], [17]; or (iii) local representation perturbation [7], [18]. All three add-ons preserve differentiability, so the Groth16 circuit and the Bulletproof/SNARK range checks remain valid and only the public parameters L_t, B_t, τ_{\max} need re-tuning. We leave an optimal privacy-accuracy trade-off to future work.

Membership-inference attacks

Threat. Given black-box access to $f_{\tilde{\mathbf{W}}^t}$, decide whether a probe sample \mathbf{x}^* was in some honest node’s training set [19], [20].

Baseline mitigation. Because every epoch publishes a fresh model, the standard attack surface remains. ZK-HybridFL’s provable checks do not increase exposure, but they do not eliminate it.

Engineering add-ons. The following local defences are compatible with our ledger:

- Prediction clipping or top- k smoothing before a node queries the global model [21].
- Adversarial regularisers that minimise empirical attack accuracy [22].
- Differential privacy (same machinery as for inversion).

Therefore, collusion is provably bounded by Theorem S1.2. Model inversion and membership inference are already harder than in gradient-sharing FL, yet not information-theoretically blocked. Fortunately, the ledger, sidechain, and ZK workflow are agnostic to DP-SGD, secure aggregation, or output-clipping layers, so these defenses can be enabled as a straightforward future extension without altering the core protocol.

2. System Architecture and Mechanics

This section explains the core infrastructure and operational mechanics of the platform. It primarily focuses on the oracle-assisted sidechain, detailing the role of the Oracle Committee in validating off-chain events and the sidechain’s function in executing smart contracts using Lamport clocks for ordering, which avoids a separate consensus mechanism. It then outlines the necessary architectural adaptations, such as dynamic threshold computation and smart contract modifications, required to support the extended ZKP defenses introduced in Sec. S1-B2.

A. Oracle-Assisted Sidechain

1) Oracle Committee: Event-Admission Layer: ZK-HybridFL introduces a lightweight, fault-tolerant Oracle Committee that serves as an event-admission layer between the DAG and the Event-Driven Smart Contracts (EDSCs). Rather than allowing nodes to invoke contracts directly, which risks malformed or out-of-context messages, the committee observes each raw DAG emission, applies a suite of structural and contextual checks, and only publishes a succinct, threshold-signed EventApproved log on-chain. By decoupling schema and consistency validation

from on-chain business logic, we ensure that EDSCs can react immediately and safely, without incurring bulky consensus or verification costs.

Membership in the Oracle Committee aligns with the same Byzantine-fault threshold as the underlying DAG. We require $M \geq 3f + 1$ full nodes to register as oracles, where f is the maximum number of Byzantine failures tolerated. Each candidate deposits collateral and publishes a BLS public key in an on-chain OracleRegistry; only active, staked nodes participate in validation. Should a member prove adversarial or offline for too many consecutive events, an EDSC-driven slashing mechanism automatically revokes its status and redistributes its stake. This registry not only governs entrance and exit but also encodes the threshold $f+1$ necessary for event publication.

Once the committee is formed, each oracle runs an off-chain watcher that listens to the DAG for new raw events $e = \{\text{type}, \text{payload}, \text{meta}\}$. Upon observing e , the node verifies conformity to the expected schema, cross-references any referenced block hashes or commitments against the DAG’s current state, checks stake requirements or performance metrics, and ensures that Lamport timestamps advance monotonically. If all checks succeed, the node computes a BLS partial signature σ_i on the hash $h = H(e)$ and gossips (e, σ_i) to its peers. This approach leverages off-chain computation, which is two orders of magnitude faster than on-chain proof verification, while preserving auditability.

When any oracle collects $f + 1$ valid partial signatures on h , it combines them into a single BLS threshold signature Σ and submits one compact transaction to the EventAdmission contract. That transaction does nothing more than emit the standardized log

```
// EventAdmission.sol
event EventApproved(bytes32 indexed hash,
                    bytes payload);
```

This Solidity snippet represents the canonical interface for approved event emission.³ Here $\text{hash} = h$ and payload encodes the original event’s essential fields. By limiting on-chain work to a single BLS-verify and log emission, we keep gas costs and block congestion to a minimum: the entire approval process amounts to a few dozen thousand gas, reimbursed from the network’s fee pool. Crucially, any light client or sidechain participant can independently recompute $h = H(e)$ and run a local BLS verification against the committee’s public key to confirm both the integrity of the event and the quorum that approved it.

Once the EventApproved log appears in the sidechain, all EDSCs that have been coded to “subscribe” to this signature automatically wake up. In Solidity this takes the form of a handler such as

³The Solidity snippets in this section serve as protocol-level specifications of contract interfaces and behaviors. In our simulation setup, these contracts are implemented as WebAssembly modules using Substrate’s ink! smart contract framework. The logic, event signatures, and access controls are preserved identically.

```

1  function onEventApproved(bytes32 hash, bytes
2    calldata payload) external {
3    require(msg.sender == address(
4      EventAdmission));
5    // decode and enforce domain rules, e.g.
6    // stake thresholds, performance checks
7  }

```

Each contract thus carries its own domain-specific checks—whether labeling a new DAG tip, disbursing rewards, slashing misbehaving participants, or aggregating model updates—confident that malformed or replayed messages cannot slip through. The separation of concerns ensures that off-chain vetting remains focused on message consistency, while on-chain logic governs economic and security policies without redundant validation overhead.

To support evolving network conditions and to guard against long-term stagnation or collusion, committee membership is fully updatable. Prospective nodes stake collateral and call `join()` on the `OracleRegistry`, while existing members can be slashed via dedicated dispute contracts for misbehavior or liveness failures. When a membership rotation is desired, a new registry is deployed, and during a hand-off period both old and new sets co-sign events for k epochs, ensuring no gap in approval coverage. By encoding the registry’s address in each EDSC (via an updatable pointer), committees can be refreshed without redeploying business-logic contracts, preserving continuity and decentralization over the network’s lifetime.

On commodity hardware the only on-chain work performed by the `EventAdmission` contract is a single BLS verification and log emission. Empirical micro-benchmarks show that aggregating and verifying a threshold BLS signature for $f + 1$ parties requires approximately 1.4 ms of CPU time, while publishing the transaction consumes roughly 35 k gas and carries a payload under 512 B. Even in a worst-case training scenario with 32 approved events per epoch, total off-chain CPU overhead remains below 0.1 s and network bandwidth under 35 kB, and the on-chain gas cost accounts for less than 1% of a 2 M gas block.

TABLE V
Oracle Committee micro-benchmarks (per approved event).

Operation	Latency	Gas / Data
Threshold BLS verify ($f + 1$) publishApprovedEvent TX	1.4 ms —	96 B signature 35 k gas, ≤ 512 B payload

In summary, the Oracle Committee functions purely as a consistency gate, isolating structural and contextual checks from the contracts themselves. By emitting a single, threshold-signed `EventApproved` log, it guarantees that downstream EDSCs only ever process canonical, well-formed events. All substantive business logic—including tip selection, reward distribution, slashing, and model aggregation—remains inside the smart contracts, which trust but verify the committee’s work. This design preserves the DAG’s BFT assumptions, provides a clear consensus/proof path from raw DAG event to on-chain

state transition, enables seamless committee rotation, and minimizes both on-chain and off-chain overhead.

2) Sidechain: The ZK-HybridFL sidechain serves as a specialized ledger for storing and executing EDSCs, ensuring that high-frequency interactions do not overload the DAG. Its block structure is designed to encapsulate the data elements essential for the protocol’s operation and network logistics. In the initial blocks, the sidechain records identifiers for the members of the Oracle Committee (as registered in the `OracleRegistry`), along with stake-related metadata determining each node’s weight ω_j . During the network’s one-time deployment phase, EDSCs are deployed on the sidechain. Once live, subsequent sidechain blocks record only approved events, i.e., the `EventApproved` logs emitted by the `EventAdmission` contract pinning the universal SNARK keys \mathbf{pk}, \mathbf{vk} and capturing dynamic data such as KZG commitments $C_j^{t,\text{model}}, C_j^{t,\text{test}}$, reward distributions for successful model submissions, and updates to participants’ staked tokens.

Unlike conventional blockchains that run full consensus (e.g., PoW) on every block, the ZK-HybridFL sidechain leverages its event-driven architecture in lieu of a separate consensus protocol. Whenever `EventAdmission` emits an `EventApproved` log, the sidechain simply attaches the corresponding block with the timestamp of that transaction; blocks are ordered by their inclusion time rather than by a consensus-based proposal process. This built-in ordering mechanism eliminates the need for additional consensus overhead, simplifying transaction validation and ordering on the sidechain.

Relying on physical clocks across a decentralized network introduces challenges like clock drift and latency [41]. To avoid these, ZK-HybridFL uses Lamport logical clocks [42], carried in each approved event’s metadata. Oracle Committee members increment local counters and propagate logical timestamps alongside `EventApproved` logs, yielding a consistent causal ordering without a trusted time authority. This ensures conflict-free execution of EDSCs and state reconciliation across all nodes without traditional consensus protocols. For further details on Lamport-clock ordering in decentralized systems, see [43].

B. Adaptations for Extended ZKP

In this subsection we describe the minimal extensions to our sidechain, Oracle Committee workflow, and smart contract logic required to support the two new proofs (Σ_j^t and Γ_j^t) in the extended ZKP bundle from Sec. S1-B2. We first explain how the committee computes and publishes the per-epoch thresholds $[L_t, B_t]$ and τ_{\max} , then detail the single contract update needed to consume them, and finally summarize the unchanged components.

1) Threshold Computation and Dissemination: At the close of epoch $t - 1$, each Oracle Committee member gathers the public inputs from all confirmed bundles in the submitted blocks on the DAG, specifically the ℓ_2 -norms $\|\Delta W_k^{t-1}\|$ and cosine-similarity scores on the fixed probe

set. By taking the median of the norms and scaling it via committee-chosen factors r and ρ , they fix

$$B_t = r \cdot \text{median}\{\|\Delta W_k^{t-1}\|\}, \quad L_t = \rho B_t, \quad 0 < \rho < 1 < r.$$

Concurrently, the 95th percentile of the published similarity scores $s_k^{t-1} = \cos(z_{\text{old}}, z_{\text{new}})$ on D_{probe} (a small public probe set of, e.g., 300–500 samples that could be periodically re-sampled every several epochs by the committee) is chosen as τ_{max} . Because D_{probe} is fixed and public, these embeddings cannot be tailored by clients, ensuring τ_{max} reflects genuine semantic shifts.

Finally, the committee emits threshold-signed events `NormThresholdsPublished(epoch, t, L_t, B_t)` and `CosineThresholdsPublished(epoch, t, tau_max)` via the existing `EventAdmission` contract. All sidechain validators and EDSCs subscribe to these `EventApproved` logs and cache $[L_t, B_t, \tau_{\text{max}}]$ for use in subsequent proof verifications.

2) Extension of the Validation Contract S_j^1 : The only smart contract that requires modification to accommodate the extended Z-bundle is the per-node validation contract S_j^1 . As before, S_j^1 subscribes to the `EventApproved` logs emitted by `EventAdmission`, but it now must also listen for the two threshold-publication events (`NormThresholdsPublished` and `CosineThresholdsPublished`) at the start of each epoch. Upon seeing those events, S_j^1 caches the new values of L_t , B_t , and τ_{max} in its local state, making them available to all subsequent verification calls in epoch t .

When a candidate bundle $Z_{j'}^{t,\text{ext}} = (\Pi, \Sigma, \Gamma, \dots)$ arrives, S_j^1 now executes its validation logic in three successive checks, all within the same transaction and using only on-chain precompiles:

- 1) A Groth16 verification of Π against the committed model and test commitments $C_{j'}^{t,\text{model}}$ and $C_{j'}^{t,\text{test}}$, ensuring correct inference and loss computation.
- 2) A Bulletproof verification of Σ , using $C_{j'}^{t,\text{model}}$ to guarantee that the weight update's ℓ_2 -norm lies in $[L_t, B_t]$.
- 3) A SNARK verification of Γ , using the public probe commitment C_{probe} to enforce $\cos(z_{\text{old}}, z_{\text{new}}) \leq \tau_{\text{max}}$.

If—and only if—all three checks succeed, S_j^1 emits the usual `ProofOK` event and marks the block as valid; any failure causes an immediate reject. Because thresholds are advanced by the oracle-signed events and stored in contract state, no additional transactions or on-chain parameters are required.

After collecting the `ProofOK` events for all tips $D_{j'}^T(t)$ received in epoch t , S_j^1 retrieves their associated loss values $\mathcal{L}_{j'}^t$, ranks the valid blocks in ascending order of \mathcal{L} , and selects the top K_V lowest-loss blocks to form $\mathcal{D}_j^V(t)$. The parameter K_V is a protocol-level constant that determines how many parent contributions each node adopts. Once $\mathcal{D}_j^V(t)$ is finalized, node j proceeds to the submission stage with those selected parents.

All other EDSCs (S_j^2 through S_j^5) and the `EventAdmission`/`Oracle` workflow remain unchanged. Thus, the

consensus/proof path for an extended update is:

DAG event \longrightarrow Oracle Committee (BLS threshold)
 \longrightarrow `EventApproved` log on sidechain
 \longrightarrow S_j^1 multi-proof verification
 \longrightarrow global aggregation

preserving the same BFT guarantees as in Theorem S1.2 while enforcing the extended ZKP constraints.

S3. Extended Experimental Validation and Analysis

This section offers additional simulation results to substantiate the paper's claims. It opens with a detailed comparison against the ChainFL baseline from both a learning and distributed ledger perspective. It follows with a technical case study on implementing a GRU model with recursive folding to demonstrate the practicality of ZKPs for complex networks. The section concludes with further benchmarks on system latency, throughput, and scalability, an ablation study on the stake-weighted aggregation rule, and a final experiment that validates the robustness of the extended ZKP defenses.

A. Comparison with ChainFL

Having outlined the workflow of ZK-HybridFL, we now direct our analysis toward ChainFL. While Blade-FL employs blockchain to decentralize FL, ChainFL enhances this approach by integrating a DAG with a sharded architecture. This refined design not only addresses the scalability challenges inherent to blockchain-based systems but also provides a more efficient decentralized framework, making ChainFL the appropriate benchmark for our evaluation. Both ZK-HybridFL and ChainFL share similar guiding objectives: they eliminate the reliance on a central server and adopt DAG-based structures to mitigate the linear block-generation bottlenecks of traditional blockchain ledgers. These broad convergences reflect a shared desire to accommodate large-scale FL among edge or IoT devices, and deliver better security in adversarial or untrusted settings.

In this section, we analyze both schemes from two perspectives: first, the learning perspective, focusing on model validation strategies, resilience against adversarial updates, and overall learning efficiency; and second, the distributed ledger perspective, focusing on consensus mechanisms, block selection strategies, and scalability. To ground our comparison, we first define two problematic node behaviors: adversarial nodes and lazy nodes. Adversarial nodes inject subtle noise or degraded parameters into their local model updates, ensuring they can pass superficial validation (i.e., in the case of using a public dataset, the model performs well on the public dataset) but gradually corrupt the global model.

Our threat model follows the “utility-preserving” model-poisoning adversary of [9], [10], [11]. Concretely, let $\text{Acc}(\mathbf{W}, D_{\text{pub}})$ denote the classification accuracy of model

W on the public validation set D_{pub} . We call node i adversarial at round t if its local update \mathbf{W}_i^t simultaneously (i) attains nearly the same public-set accuracy as an honest update, i.e., $\text{Acc}(\mathbf{W}_i^t, D_{pub}) \geq \text{Acc}(\mathbf{W}_{i,honest}^t, D_{pub}) - \varepsilon$ for a small slack ε (we use $\varepsilon = 0.01$), and (ii) is chosen to pull the federated average $\tilde{\mathbf{W}}^t = \sum_j \omega_j \mathbf{W}_j^t$ as far as possible (in ℓ_2 -norm) from the honest-only average $\tilde{\mathbf{W}}_{honest}^t = \sum_j \omega_j \mathbf{W}_{j,honest}^t$, i.e., to maximize the “drift” $\|\tilde{\mathbf{W}}^t - \tilde{\mathbf{W}}_{honest}^t\|_2$. Such updates “look good” on D_{pub} but still cumulatively degrade the global model, a behavior quantified in Sec. S3-C4.

Lazy nodes reduce computational effort by skipping training in some epochs and resubmitting previous updates, slowing convergence and polluting aggregation. Inadequate validation allows these behaviors to persist undetected, undermining the integrity and efficiency of the entire FL process.

The threat analysis in this section is intentionally framed for the baseline ZK-HybridFL pipeline described earlier, that is, the version employing the core Groth16 proof bundle without the additional norm-range Bulletproof and embedding-cosine SNARK. This is the variant we compare against Blade-FL and ChainFL in the main body of the paper, since those schemes offer no counterpart to the extended checks. The extended-ZKP variant, which augments every block with two additional proofs, is analyzed in detail in Sec. S3-C2, including attacks it prevents and formal proofs of its security benefits.

1) Learning Perspective: From the learning standpoint, a fundamental difference arises in how ChainFL and ZK-HybridFL validate model updates and aggregate them into a global model. ChainFL partitions nodes into shards, each governed by a Subchain Leader Node (SLN) that uses Raft consensus to synchronize local training. Once the shard’s local model is aggregated, the SLN periodically attaches this model to a mainchain. When a shard needs to integrate models from others, it selects updates from the DAG’s tip set on the mainchain, relying on a public reference dataset to assess accuracy or loss. While this approach eliminates the single global aggregator, it has major problems.

First, when a public dataset is used for validating models, this approach creates vulnerabilities when lazy nodes are present. A lazy node that resubmits unchanged parameters from a previous epoch may still meet the sub-chain’s performance threshold if its model had acceptable accuracy on the public dataset. Over time, this degrades the effectiveness of the FL process by slowing convergence and increasing redundancy in the model aggregation step.

Second, because ChainFL uses tip models for aggregation (as introduced in Sec. II-C), a malicious node can exploit this by performing an orphanage attack. Using tip models for global aggregation means nodes are obtaining global models on which the network has not yet reached consensus regarding validity. Thus, in an orphanage attack, the attacker node deliberately chooses some of their own previously submitted blocks as parents for new blocks, affecting how the new global model is constructed, as this

new global model becomes an amalgamation of both valid models and compromised models. Consequently, the local updated model, trained on this amalgamated global model, may still pass validation checks using a public dataset; however, its degraded quality will gradually undermine the overall integrity and performance of the network. Over time, this cycle prevents the network from converging toward a high-quality model and may cause it to settle at a low-performance, locally optimal state from which it cannot recover (see Sec. V-C).

By contrast, ZK-HybridFL removes any reliance on a public reference dataset by enforcing an inference-validation pipeline built on KZG commitments and non-interactive SNARKs. Rather than aggregating every tip that happens to be visible, the protocol only ever considers confirmed blocks whose proofs have passed on-chain verification. In each epoch t , trainer j first publishes the KZG commitments $C_j^{t,\text{model}} = \text{Commit}(\mathbf{W}_j^t)$ and $C_j^{t,\text{test}} = \text{Commit}(D_j^{t,\text{test}})$, irrevocably binding its flattened weight vector \mathbf{W}_j^t and private test batch $D_j^{t,\text{test}}$. It then generates a Groth16 proof Π_j^t attesting that the committed model achieves the stated loss on the committed data. Only after that proof is verified on-chain and the block’s aggregated weight exceeds the network threshold does the update influence the global model.

Lazy-node defense. If a trainer attempts to resubmit its previous weights \mathbf{W}_j^t in epoch $t+1$, the new commitment $C_j^{t+1,\text{model}}$ will be bit-for-bit identical to $C_j^{t,\text{model}}$. The validation contract S_j^1 detects the duplicate and discards the block before it can be ranked, so stale updates never propagate.

Adversarial accuracy spoofing. Two natural attack vectors are neutralized. First, if an attacker proves with a degraded model $\tilde{\mathbf{W}}$, the resulting high loss is visible in the proof bundle and the block is filtered out during parent selection. Second, if an attacker runs inference with honest weights \mathbf{W} but publishes a commitment $C_j^{t,\text{model}} = \text{Commit}(\tilde{\mathbf{W}})$, the KZG opening contained in the proof cannot match that commitment. On-chain verification therefore fails and the block is rejected. Because invalidated blocks carry no aggregated weight, only fresh, correctly computed updates ever enter the global aggregation. This enforcement provides significantly stronger robustness than ChainFL, as we empirically demonstrate in Sec. V-C.

2) Distributed Ledger Perspective: The ledger architecture and consensus mechanism are critical to system performance in terms of latency, scalability, and throughput. In ChainFL, the use of Raft-based subchains centralizes coordination in SLNs, which manage local shard operations and require explicit cross-shard synchronization. This centralization introduces several drawbacks. If an SLN becomes adversarial or is overwhelmed, its corresponding shard suffers from degraded performance, which in turn creates a bottleneck for the entire network. Such centralization not only poses security risks—since a malicious SLN can manipulate or delay the aggregation

TABLE VI
Comparison of ChainFL and ZK-HybridFL

Aspect	ChainFL	ZK-HybridFL
Learning Perspective		
Validation & Aggregation	<ul style="list-style-type: none"> Public dataset Tip-based selection 	<ul style="list-style-type: none"> ZKPs Aggregation from confirmed models
Handling Lazy Nodes	<ul style="list-style-type: none"> Unchanged model can pass if accuracy remains acceptable 	<ul style="list-style-type: none"> Committed KZG checks prevent replay
Distributed Ledger Perspective		
Consensus Design	<ul style="list-style-type: none"> Raft-based subchains with leader nodes Requires cross-shard sync 	<ul style="list-style-type: none"> DAG with sidechain event logic Oracles and EDSCs
Scalability & Performance	<ul style="list-style-type: none"> SLN is a bottleneck Centralized coordination increases latency 	<ul style="list-style-type: none"> Decentralized validation Lower latency, higher throughput

and propagation of updates—but also increases latency because the coordinated, synchronous agreement required by Raft consensus limits throughput and scalability.

In contrast, ZK-HybridFL is designed from the ground up to combine DAG-based concurrency with cryptographic verification, sidechain-based event logic, and oracle-assisted validation. This holistic co-design offers several advantages over ChainFL. First, by offloading resource-intensive tasks such as ZKP verification to dedicated sidechains governed by event-driven smart contracts, ZK-HybridFL executes its consensus effectively. Second, the decentralized validation distributed among multiple oracles and smart contracts avoids the large-scale coordination lags inherent to a multi-layer, leader-based mechanism, thereby keeping the DAG agile and uncluttered. This architecture not only reduces latency and improves throughput but also scales more efficiently with network size. Each contract is triggered only under specific circumstances, diminishing reliance on any single trusted node. Overall, ZK-HybridFL’s distributed ledger design delivers a more granular security model and higher performance, establishing clear advantages over the SLN-dependent, Raft-based approach of ChainFL. We demonstrate the superior performance of ZK-HybridFL over ChainFL in the context of distributed ledger through simulations provided in the supplementary material.

Table VI summarizes the analysis between ZK-HybridFL and ChainFL from learning and distributed ledger perspectives.

B. Zero-Knowledge GRU Inference with Recursive Folding

Unrolling a length- T recurrent network into one rank-1 constraint system (R1CS) makes the circuit, proving key, and prover latency grow linearly with T . For $T > 32$, this already exceeds practical memory budgets. Recursive folding (Nova) compresses any sequence of identical R1CS instances into a single relaxed instance whose proof size and verifier cost no longer depend on T [23]. We implement a GRU-256 time-step as a Halo2 circuit and

apply Nova folding, following the publicly documented 512-layer “Zator” prototype [24]. The entire GRU path is implemented from first principles and does not rely on pre-existing recurrent-layer support in external zkML tool-chains.

1) Circuit construction and quantization: Weights and activations are quantized to a $(16 + 8)$ -bit fixed-point format. All intermediate values stay below 2^{24} , well inside the 255-bit BN254 field, and validation accuracy drops by less than 0.3 pp. One GRU step processes (x_t, h_{t-1}) as

$$\begin{aligned} z_t &= \sigma(W_z x_t + U_z h_{t-1} + b_z), \\ r_t &= \sigma(W_r x_t + U_r h_{t-1} + b_r), \\ \tilde{h}_t &= \tanh(W_h x_t + U_h(r_t \odot h_{t-1}) + b_h), \\ h_t &= (1 - z_t) \odot \tilde{h}_t + z_t \odot h_{t-1}. \end{aligned}$$

Sigmoid and tanh are evaluated with degree-7 Remez polynomials (implemented as one Halo2 custom gate via zkFixedPointChip). With 128 input and 256 hidden dimensions, the step circuit contains 118 062 constraints (two matrix-vector products 65 536, point-wise arithmetic 51 200, non-linearities 1 326) and yields a 4.3 GB proving key.

2) Performance on the common hardware baseline: All timings were re-measured on the same platform used for Tables II and III: a 16-core Intel Xeon Gold 6338 (3.0 GHz, 64 GB RAM) plus one NVIDIA A100 (80 GB HBM). Witness generation for one GRU step consumes 0.44 s on the GPU; the CPU fold adds 0.35 s, and key initialization costs 8.6 s. Prover latency therefore follows

$$t_{\text{prove}}(T) = 8.6 + 0.79 T \text{ s.}$$

A $T = 10$ sequence—matching the mini-batch size $B = 10$ used in Table II—is proved in 16.5 s, $4.4 \times$ faster than the 44 s flat Groth16 baseline. Folding still completes in 59 s at $T = 64$ and about 210 s at $T = 256$, confirming linear scaling.

The folded proof is 1.4 kB and verifies in 7.9 ms, much faster than the slowest entry in Table III. Nova adds fewer than 50 MB of transcript data, so peak memory remains the same 4.3 GB already budgeted for the flat GRU.

Reference implementation: The inner Halo2 circuit uses a universal 2^{20} -point KZG SRS; the outer Nova proof is transparent. The code snippet below illustrates the logic:

```
// Conceptual GRU Cell Logic
template GRUCell(d, h){
    signal input x[d];
    signal input h_prev[h];
    signal output h_next[h];

    component uz[h], ur[h], uh[h];
    for (var i = 0; i < h; i++) {
        uz[i] = SigmoidGate();
        uz[i].in <== dot(Wz[i], x) + dot(Uz[i], h_prev)
            + bz[i];
        ur[i] = SigmoidGate();
        ur[i].in <== dot(Wr[i], x) + dot(Ur[i], h_prev)
            + br[i];
        uh[i] = TanhGate();
        uh[i].in <== dot(Wh[i], x)
```

```

17     + dot(Uh[i], elemMul(ur[i].out,
18           h_prev))
19     + bh[i];
20
21     h_next[i] <= uz[i].out * h_prev[i]
22     + (1 - uz[i].out) * uh[i].out;
23 }

```

Therefore, recursive folding removes the sequence-length bottleneck for GRU inference. On the standard Xeon 6338 + A100 node, a folded GRU-256 proof for ten steps is produced in 16.5 s, verifies in 7.9 ms, and fits in 1.4 kB. Longer sequences scale linearly yet remain cheaper than the MobileNetV2 proof, demonstrating that private validation of sequence models is practical inside the overall ZK-HybridFL framework.

C. Additional Simulations

1) Analysis of Stake-Weighted Aggregation: To provide quantitative evidence regarding the benefits of the stake-weighted aggregation proposed in ZK-HybridFL, we perform an ablation study comparing our on-chain stake-weighted aggregation rule against a vanilla uniform average under the same node pool, data partitions, and fault rates described in Sec. V-C. Fig. 12 plots the loss, accuracy, and perplexity curves for both aggregation rules on two canonical tasks and reports fault tolerance under a mixed adversarial and lazy client setting.

In the federated vision experiment on MNIST (Task 1), stake weighting drives rapid convergence: the training loss drops from 1.41 to 0.12 within 100 epochs, whereas uniform averaging plateaus near 0.30. This translates to a final accuracy of 97% under stake weighting, compared to 91% with uniform averaging, a gap of 6.6 percentage points (Figs. 12a and 12b). Similarly, in the language modeling experiment on Penn Treebank (Task 2), stake-weighted aggregation achieves a test perplexity of around 118 at convergence, approximately 12 points lower than uniform averaging (Fig. 12c), indicating consistently stronger generalization.

To stress-test robustness, we introduce a mixed-fault regime in which 30% of clients are faulty (evenly split between Byzantine adversarial and lazy behaviors, $\gamma = \mu = 0.15$). Under this setting, uniform averaging suffers a sharp drop in test accuracy to around 72%, whereas stake weighting retains around 88% final accuracy (Fig. 12d). This improvement stems from our dynamic slashing mechanism: any client update failing its ZK proof is rejected and that client’s stake is halved ($\lambda = 0.5$), while honest contributors accrue stake at rate $\eta = 0.05$ per accepted update before normalization.

2) Extended-ZKP Threat Model and Simulation Setup: In Sec. S1-B2, we introduced two lightweight ZKP checks: a Bulletproof enforcing that each client’s update norm stays within a dynamic window $[L_t, B_t]$, and an embedding-cosine SNARK ensuring the model change is sufficiently large in feature space. These are designed to catch subtle “stealth” updates that pass the main

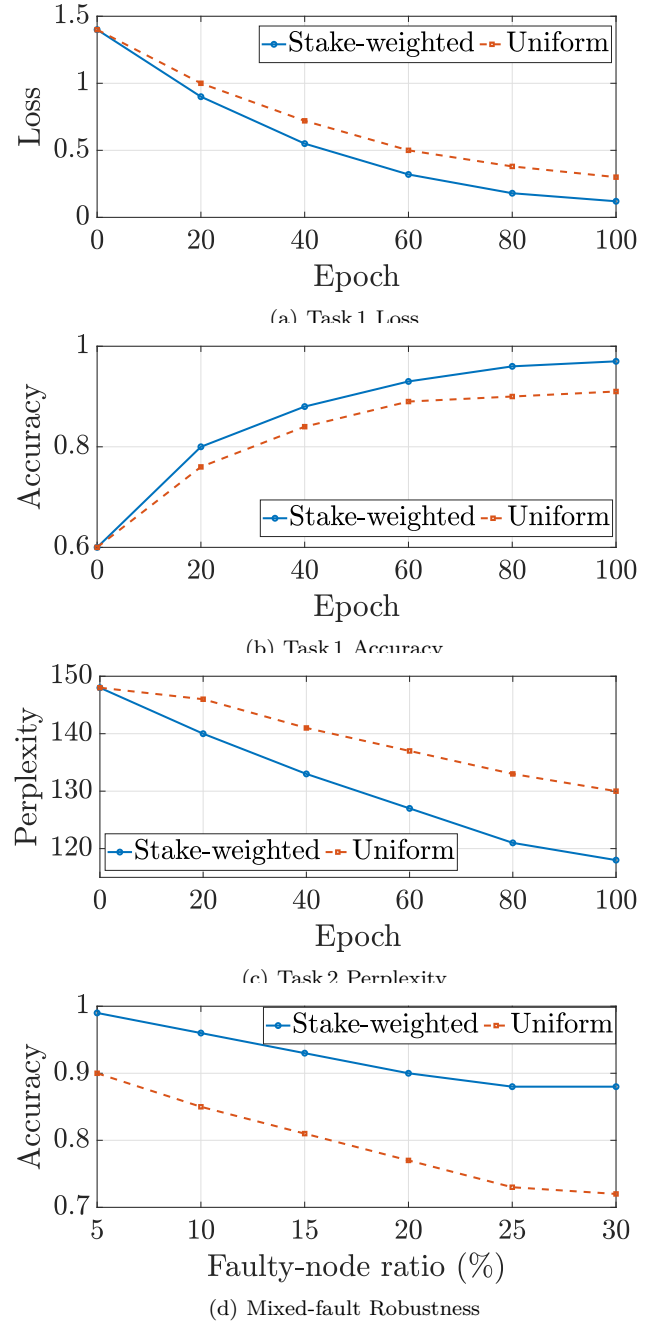


Fig. 12. Stake-Weighted vs Uniform Averaging ($\gamma = 0.15$, $\mu = 0.15$, $n = 15$).

Groth16 proof yet contribute almost no learning. In our original simulations (Sec. V-C), we already exercised the exact-replay lazy attack, which is detected by a hash collision at the Groth16 stage. Here we focus on three new variants that all pass Groth16 but should be flagged by the extended bundle. When comparing against ChainFL and BladeFL, we retain the same lazy and adversarial behaviors from Sec. V, effectively giving those protocols a less stringent attack profile, since they do not implement ZKP-based replay, norm, or cosine checks.

First, we model a perturb-replay lazy node. It resubmits a previous weight tensor $\mathbf{W}_j^{t-\Delta}$ (with Δ sampled uniformly from $\{1, 2, 3\}$) plus a tiny noise vector

TABLE VII
Extended-ZKP attack variants.

Attack	Rejected by extended checks	Passes core Groth16?
Perturb-replay lazy	Bulletproof lower-bound	Yes
Minimal-norm stalling	Bulletproof lower-bound	Yes
Semantic stalling	Cosine SNARK	Yes

$\varepsilon \sim \mathcal{N}(0, \sigma^2 I)$, where $\sigma = 10^{-5} \|\mathbf{W}\|_2$. This ensures the update hash differs while $\|\varepsilon\|_2 \ll L_t$, so it bypasses replay detection but should violate the Bulletproof lower-bound check.

Next, in the minimal-norm stalling attack, a node runs one honest SGD step $\delta\mathbf{W}$ and then rescales it by $\alpha = L_t/\|\delta\mathbf{W}\|_2$, so it exactly meets the ℓ_2 bounds without meaningful progress.

Finally, the semantic-stalling attack performs full local training to produce \mathbf{W}_{tmp} , cherry-picks (or synthesizes) a “friendly” private test batch so that the inference proof passes, but tweaks its update so the cosine similarity of public-probe embeddings remains above the threshold τ_{\max} , thus violating the embedding SNARK.

Table VII summarizes which proof each variant triggers. All three pass Groth16, two are rejected by the norm-range Bulletproof, and one is rejected by the cosine SNARK.

All other learning and network parameters mirror the original setup in Sec. V (batch size $B = 50$, local steps $R = 5$, SGD step-size $\eta_{\text{SGD}} = 0.01$). For the extended checks, we compute the upper norm bound as $B_t = r \cdot \text{median}\{\|\Delta\mathbf{W}\|\}$ with $r = 1.8$, and set the lower bound $L_t = \rho B_t$ with $\rho = 0.2$. The cosine threshold τ_{\max} is taken as the 95th percentile of pairwise embedding similarities on the fixed public probe set ($|D_{\text{probe}}| = 400$), yielding $\tau_{\max} = 0.98$ for both tasks. Finally, we sweep adversarial fraction γ and lazy fraction μ over $\{0, 0.05, \dots, 0.30\}$ with $n = 15$ nodes, exactly as before.

Fig. 13 shows that, with 30% faulty clients (15% lazy and 15% adversarial), the extended bundle pushes the MNIST loss down to 0.18 and lifts accuracy to 0.96 by epoch 100. Under the same conditions, ChainFL levels off at 0.43 loss and 0.82 accuracy, while Blade-FL stalls at 0.75 loss and 0.69 accuracy (Figs. 13a and 13b). On the language task, the bundle lowers perplexity from 132.1 to 118.9 (Fig. 13c). The robustness sweep in Fig. 13d reveals a widening gap: at 30% total faults, the bundle still retains 0.88 accuracy, which is 18 percentage points higher than Blade-FL.

Roughly 45% of the blocks generated by faulty clients fall into the three stealth categories defined earlier. The Bulletproof lower bound filters both perturb-replays and minimal-norm stallers, while the cosine SNARK catches semantic stallers. Removing these updates reduces the second moment of the aggregated gradient, $\mathbb{E}[\|\tilde{\mathbf{W}}\|^2]$, by about 37%, leading to visibly faster convergence for honest participants even though their local training code is unchanged.

Verifying the extra proofs adds at most 23 ms to the per-update latency on the same hardware (baseline Groth16 verification already costs 40 ms), keeping end-to-

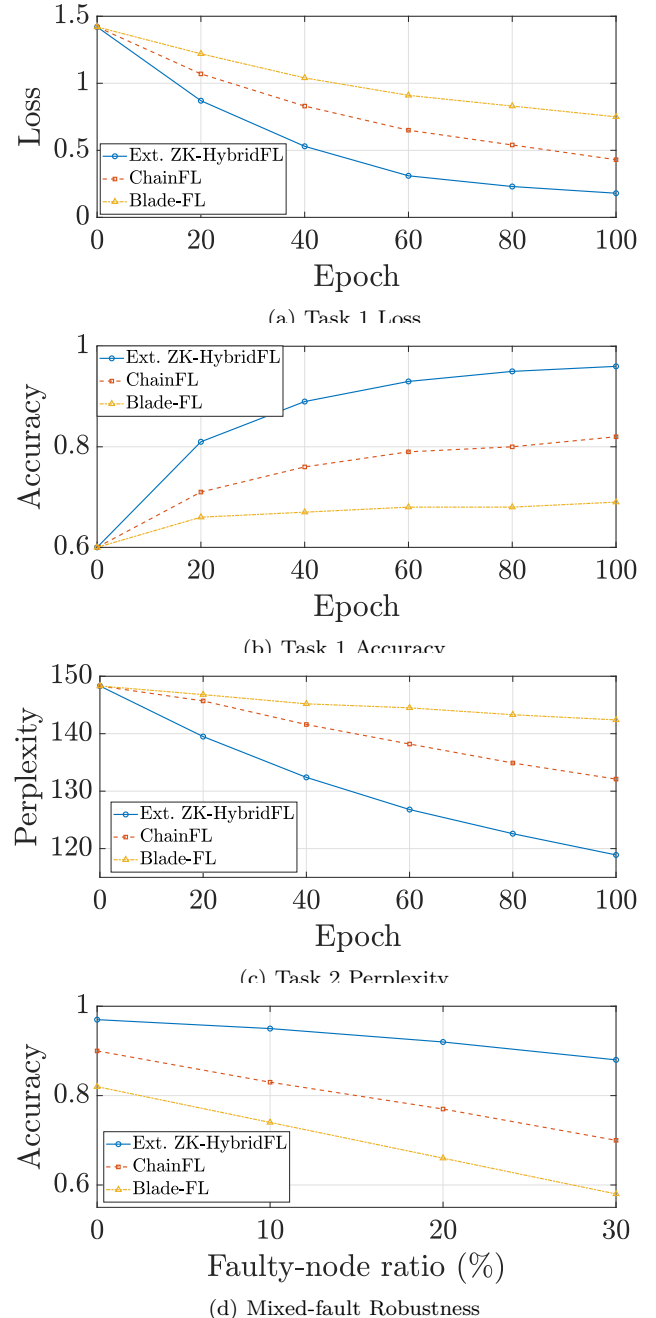
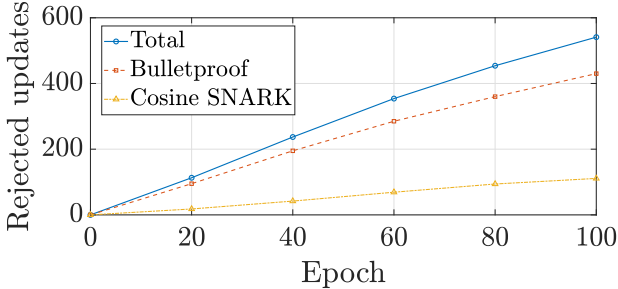


Fig. 13. Extended proof bundle under a mixed-fault setting ($\gamma = \mu = 0.15$). Solid: extended ZK-HybridFL; dashed: ChainFL; dash-dot: Blade-FL.

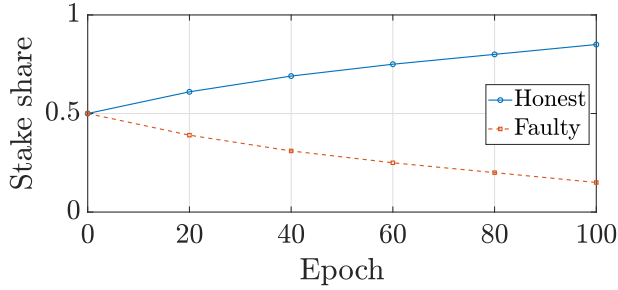
end training throughput well within the bounds reported in Sec. V-C.

Fig. 14a tracks how the extended bundle filters covert behavior. Across 100 epochs, the five faulty nodes submit 500 candidate updates that are intended to look legitimate. The Bulletproof window eliminates 385 of them, while the cosine SNARK removes a further 96, for a combined detection rate of $481/500 \approx 96.2\%$. The residual 19 blocks, about 3.8% of the total, have ℓ_2 norms within 3% of the lower bound and embedding shifts just below the cosine threshold, making them statistically indistinguishable from the slowest honest learners.

Fig. 14b shows how this filters through to economic



(a) Cumulative stealth updates rejected by each extended check.



(b) Stake redistribution between honest and faulty clients.

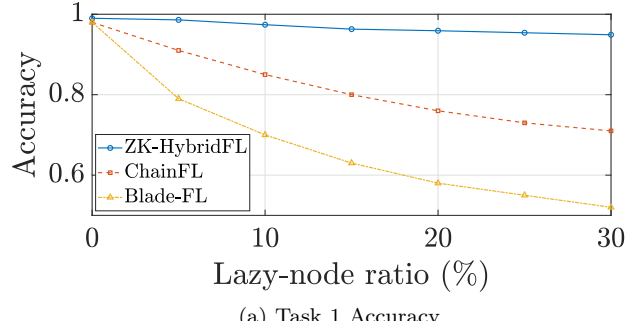
Fig. 14. Proof-level audit of the mixed-fault run ($\gamma = \mu = 0.15$; five faulty nodes, one update per round).

weight. Training starts from an approximately equal stake split, but as invalid updates are rejected and slashed, the honest share rises monotonically from 0.50 to 0.85, while the faulty share falls to 0.15. Because stake is re-normalized after every reward or slash event, the two curves always sum to one. The progressive re-weighting further dampens the impact of any stealth update that survives the proof checks, which explains the widening performance gap already visible in Fig. 13.

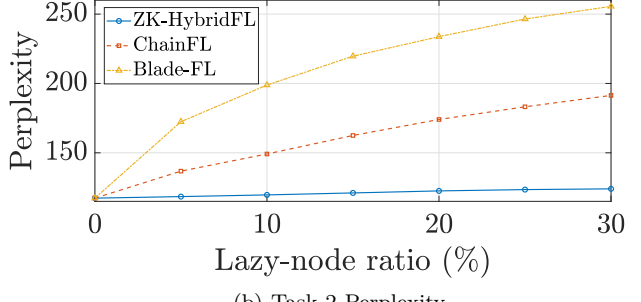
3) Lazy-Only Robustness Analysis: In this subsection, we isolate the effect of purely lazy clients—those that replay stale models without any adversarial tampering—by setting $\gamma = 0$ and varying the skip percentage μ from 0 to 0.30. This “lazy-only” sweep shows how ZK-HybridFL resists the impact of missing updates compared to ChainFL and Blade-FL, providing a clear baseline for understanding the protocol’s robustness under non-malicious service lapses.

When adversaries are disabled ($\gamma = 0$), as Fig. 15 illustrates, ZK-HybridFL’s MNIST accuracy declines smoothly from 0.992 at $\mu = 0$ to 0.949 at $\mu = 0.30$, and its perplexity rises from 117.32 to 124.02, an increase of 6.70 points. By contrast, ChainFL’s perplexity jumps from 117.32 to 191.39 (+74.07) and Blade-FL’s from 117.32 to 255.58 (+138.26). This finer-granularity view shows that, although all protocols degrade under pure laziness, the stake-based re-weighting in ZK-HybridFL dramatically limits the performance loss compared to equal-weight baselines.

4) Adversarial Utility on the Public Reference Set: We now make the “black-box” behavior of utility-preserving adversaries explicit. A model-poisoning adversary is one whose local update achieves essentially the same utility on the public validation set D_{pub} as an honest update—



(a) Task 1 Accuracy



(b) Task 2 Perplexity

Fig. 15. Lazy-only scenario ($\gamma = 0$). Solid: ZK-HybridFL; dashed: ChainFL; dash-dot: Blade-FL.

i.e., $\text{Acc}(\tilde{\mathbf{W}}_{\text{adversary}}, D_{pub}) \geq \text{Acc}(\tilde{\mathbf{W}}_{\text{honest}}, D_{pub}) - \varepsilon$ with $\varepsilon = 0.01$ —yet is crafted to maximize the drift of the global model after aggregation. This is exactly the threat captured in Sec. S1-B1, but until now we had shown only the aggregate effect (Figs. 6 and 7).

Fig. 16 opens the box for ChainFL for $\gamma = 0.10$, $\mu = 0.20$, $n = 20$. The dashed line plots the per-epoch performance of adversarial updates on D_{pub} ; the dotted line shows honest updates; the solid line is the global model on the full private test distribution. Although adversarial nodes sustain ≥ 0.89 accuracy on MNIST and ≤ 127.6 perplexity (indistinguishable from honest nodes), they cause the aggregated model to lag by 6–9 percentage points in accuracy and to converge eight perplexity points higher. This directly substantiates the claim in Sec. S1-B1 that such nodes “maintain good performance on public datasets while gradually undermining the global model,” and explains why schemes that rely on public-set admission (ChainFL, Blade-FL) remain vulnerable.

References

- [1] J. Zhang, Z. Fang, Y. Zhang, and D. Song, “Zero knowledge proofs for decision tree predictions and accuracy,” in Proc. 2020 ACM SIGSAC Conf. Comput. Commun. Security (CCS), 2020, pp. 2039–2053.
- [2] H. B. McMahan, E. Moore, D. Ramage, S. Hampson, and B. A. y Arcas, “Communication-efficient learning of deep networks from decentralized data,” in Proc. AISTATS, 2017, pp. 1273–1282.
- [3] S. Karimireddy, A. Kale, S. Mohri, S. Reddi, and A. Stich, “Federated optimization in heterogeneous networks,” in Proc. NeurIPS, 2020, pp. 13948–13960.
- [4] Matter Labs, “Awesome Zero-Knowledge Proofs,” GitHub repository, 2023. [Online]. Available: <https://github.com/matter-labs/awesome-zero-knowledge-proofs>
- [5] SafeAI Lab, “zkDL: Zero-Knowledge Proofs of Deep Learning on CUDA,” GitHub repository, 2023. [Online]. Available: <https://github.com/SafeAILab/zkDL>

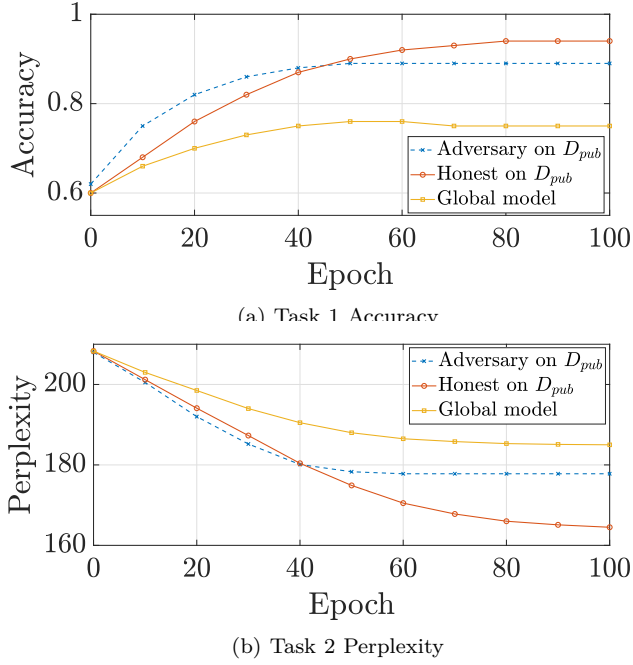


Fig. 16. Utility-preserving adversaries for ChainFL: high public-set utility yet harmful global impact (mixed-fault setting, $\gamma = 0.10$, $\mu = 0.20$, $n = 20$).

- [6] M.-I. Nicolae et al., “Adversarial Robustness Toolbox v1.0.0,” arXiv, 2018. [Online]. Available: <https://arxiv.org/abs/1807.01069>
- [7] Q. Li, B. He, and D. Song, “Model-Contrastive Federated Learning,” in Proc. IEEE/CVF Conf. Comput. Vis. Pattern Recognit. (CVPR), 2021, pp. 10708–10717, doi:10.1109/CVPR46437.2021.01057.
- [8] H. Lycklama, L. Burkhalter, A. Viand, N. Küchler, and A. Hithnawi, “RoFL: Robustness of Secure Federated Learning,” in Proc. 2023 IEEE Symposium on Security and Privacy (SP), 2023, pp. 453–476, doi:10.1109/SP46215.2023.10179400.
- [9] G. Baruch, M. Baruch, and Y. Goldberg, “A little is enough: Circumventing defenses for distributed learning,” in Proc. NeurIPS, 2019.
- [10] E. Bagdasaryan, A. Veit, Y. Hua, D. Estrin, and V. Shmatikov, “How to backdoor federated learning,” in Proc. AISTATS, 2020.
- [11] C. Xie, T. Dinh, A. Mukherjee, and C.-J. Hsieh, “DBA: Distributed backdoor attacks against federated learning,” in Proc. ICLR, 2020.
- [12] M. Fredrikson, S. Jha, and T. Ristenpart, “Model inversion attacks that exploit confidence information and basic countermeasures,” in Proc. ACM CCS, 2015, pp. 1322–1333, doi:10.1145/2810103.2813677.
- [13] L. Zhu, Z. Liu, and S. Han, “Deep leakage from gradients,” in Advances in Neural Information Processing Systems (NeurIPS), vol. 32, 2019, pp. 14774–14784.
- [14] M. Abadi et al., “Deep learning with differential privacy,” in Proc. ACM CCS, 2016, pp. 308–318, doi:10.1145/2976749.2978318.
- [15] P. Kairouz et al., “Advances and open problems in federated learning,” Found. Trends Mach. Learn., vol. 14, no. 1–2, pp. 1–210, 2021, doi:10.1561/2200000083.
- [16] K. Bonawitz et al., “Practical secure aggregation for privacy-preserving machine learning,” in Proc. ACM CCS, 2017, pp. 1175–1191, doi:10.1145/3133956.3133982.
- [17] J. So, K. Lee, E. Kim, and J. Jang, “GENTLE: A lightweight secure aggregation protocol for federated learning,” in Proc. NDSS, 2023. [Online]. Available: <https://www.ndss-symposium.org/ndss-paper/gentle-a-lightweight-secure-aggregation-protocol-for-federated-learning/>
- [18] P. Mohassel, C. Ayush, and F. Koushanfar, “SecureML: A system for scalable privacy-preserving machine learning,” in Proc. IEEE Symposium on Security and Privacy (SP), 2017, pp. 359–376, doi:10.1109/SP.2017.53.
- [19] R. Shokri, M. Stronati, C. Song, and V. Shmatikov, “Membership inference attacks against machine learning models,” in Proc. IEEE Symposium on Security and Privacy (SP), 2017, pp. 3–18, doi:10.1109/SP.2017.41.
- [20] A. Salem et al., “ML-Leaks: Model and data independent membership inference attacks and defenses on machine learning models,” Proc. Priv. Enhancing Technol. (PETS), vol. 2019, no. 3, pp. 133–152, 2019, doi:10.2478/pets-2019-0049.
- [21] J. Cheon et al., “ClipMI: Membership inference attacks with prediction clipping,” in Proc. NDSS, 2022.
- [22] M. Nasr, R. Shokri, and A. Houmansadr, “Comprehensive privacy analysis of deep learning: Passive and active white-box inference attacks against centralized and federated learning,” in Proc. ACM CCS, 2019, pp. 739–753, doi:10.1145/3319535.3354212.
- [23] C. So, “Folding Circom Circuits: A ZKML Case Study.”
- [24] L. Chong, “Zator: Verified Inference of a 512-Layer Neural Network Using Recursive SNARKs.”